NCAR/CT-51
INSTAAR/OP-28
ISSN 0004-6145

Tropical Teleconnections to the Seesaw in Winter Temperatures between Greenland and Northern Europe

Gerald Allen Meehl

NCAR Cooperative Thesis No. 51
INSTAAR Occasional Paper No. 28

Institute of Arctic and Alpine Research, University of Colorado, and
National Center for Atmospheric Research

1978

NCAR/CT-51
INSTAAR/OP-28
ISSN 0004-6145

Tropical Teleconnections to the Seesaw in Winter Temperatures between Greenland and Northern Europe

Gerald Allen Meehl

A thesis submitted to the Graduate School of the University of Colorado in partial fulfillment of the requirements for the degree of Master of Arts, Department of Geography, based on research conducted in cooperation with the scientific staff of the Empirical Studies Group of the Climate Section, Atmospheric Analysis and Prediction Division, National Center for Atmospheric Research, Boulder, Colorado.

Mr. Meehl received his B.A. degree from the University of Colorado in 1974.

NCAR Cooperative Thesis No. 51
INSTAAR Occasional Paper No. 28

Institute of Arctic and Alpine Research, University of Colorado, and
National Center for Atmospheric Research

1978

ABSTRACT

A prominent feature of inter-annual variability in middle and high latitudes is the so-called "Greenland Seesaw", the well-known tendency for winter temperatures to be low over northern Europe when they are high over Greenland (GA), and vice versa (GB). Well-defined mean pressure anomalies over the North Pacific, America, North Atlantic, and Europe are associated with these temperature patterns. In this study tropical teleconnections associated with the seesaw are discussed. It has been found that the strength of mean sea-level westerlies in the central North Atlantic Ocean during seesaw winters is highly correlated with that of the northeast and southeast trades in the Atlantic, with the trades being stronger (weaker) during GB (GA) winters. Similar associations exist with the trade winds in the North Pacific. There is a statistically significant correlation between the strength of the northeast and southeast trades in the Atlantic during the seesaw winters, but not in other winters. The position of the subtropical jet at 300 mb in the Northern Hemisphere appears to move north (south) in the GB (GA) winters with the exception of a shift in the opposite sense over Africa. A southward (northward) shift in the position of the ITCZ in Africa, as defined by the belt of heaviest precipitation, is seen during the winters when Greenland temperatures are well below (above) those in northern Europe.

Relative sea levels taken across the Gulf Stream indicate that geostrophic velocity of the current decreases (increases) in the GB (GA) winters. Significantly lower (higher) sea surface temperatures exist across the tropical North Atlantic, North Pacific, and Indian Oceans during GB (GA) winters. Atmospheric-related patterns appear strongly only during seesaw winters, although small magnitude pressure anomaly patterns of the type seen during seesaw winters are present in autumns preceding those seesaw winters. Trade wind anomalies seem to persist through all seasons prior to and following seesaw winters south of 20^{o}N, with the northern fringes of the trade wind belt reacting mainly during seesaw winters. In contrast, ocean-related features associated with the seesaw occur at all latitudes in summers and autumns preceding, and springs following, seesaw winters.

ACKNOWLEDGMENTS

This work would not have been possible without the suggestions, comments, and assistance of Harry van Loon of NCAR and Roger Barry of INSTAAR. Discussions with Roland Madden, James McWilliams and Peter Gent were of great benefit. I would like to thank Roy Jenne, Will Spangler and Paul Mulder for their advice and assistance with the handling of the data. I would also like to thank Warren Washington, David Baumhefner and Robert Chervin for their understanding and encouragement throughout this endeavor. This research was supported by the National Science Foundation's Climate Dynamics Program, Climate Dynamics Research section grant #ATM-76-20508 to the Institute of Arctic and Alpine Research of the University of Colorado in Boulder.

TABLE OF CONTENTS

LIST OF TABLES

LIST OF FIGURES

Figure Page

Figure | Page

Figure | Page

Chapter 1

INTRODUCTION

"Sooner or later we shall catch the nimble imp that jeers at us today, and, if I mistake not, when he is caught we shall make him tell us something of the real secrets of these atmospheric relationships." W. N. SHAW, 1905

The problem of understanding what role tropical processes play in the general circulation of the atmosphere has long been recognized as important. In 1905 Shaw pointed out certain relationships that seemed to exist between the Southeast Trade Winds in the Atlantic and rainfall in London. He felt that studying and understanding the tropics could lead to the prediction of midlatitude weather. As he put it, it is important to "put our finger on the pulse of that endless and complex process of transformation of solar energy of which the weather of our islands [England] and elsewhere is an expression."

C. F. Brooks (1931) traced European weather fluctuations, which appeared to be strongly influenced by North Atlantic sea surface temperatures (SST's), to varying intensities of Atlantic trade wind systems and associated Gulf Stream transports. The relationships between trade wind intensities, ocean current transports, and midlatitude SST and weather patterns has recently been studied by a number of investigators in the continuing effort to identify what links the tropics have with midlatitude weather systems (e.g., Reiter, 1978). In a similar vein, several researchers have looked at tropical SST's and their relation to trade wind intensities as

being symptomatic of variations in northward transports of heat and momentum from the tropics to the midlatitudes by the Hadley Cell. The end result of this chain of events is circulation anomalies and associated global weather changes (e.g., Bjerknes, 1966; Nicholls, 1977).

There is no need to emphasize the ramifications that even a minor fluctuation of climate can have on an economy or a society. Yet, in order to predict a weather or climate anomaly, there must first be a thorough understanding of how the atmosphere as a whole works. Even a regional climate fluctuation, such as the Sahel drought, is usually indicative of a global change of circulation (Kidson, 1977). The underlying importance of understanding tropical interactions with the general circulation was dramatically underscored by Rowntree (1976) when he showed that tropical forcing in a numerical simulation was found to affect the entire circulation throughout the troposphere in middle as well as high latitudes.

It is the purpose of this study, therefore, to investigate the extent to which processes taking place in the tropics can be linked directly to a major mode of midlatitude circulation called the "Greenland seesaw" as defined by van Loon and Rogers (1978). Midlatitude links to tropical pressure and wind systems, African ITCZ precipitation, fluctuations in Gulf Stream velocity, tropical SST's, subtropical jet stream position as indicated by the upper troposphere west wind maximum, and conditions in the seasons before and after seesaw winters will be explored. Hopefully, further insight will be gained into understanding the links between the tropics and midlatitudes and their interactive role in influencing the general circulation of the atmosphere.

Chapter 2

DATA

Sea level pressure data north of 20^{o}N were taken from the NCAR $5^{o}x5^{o}$ monthly mean historical sea level pressure grid. Individual historical station data used for areas south of 20^{o}N were taken from the World Monthly Surface Climatology tape at NCAR.

The monthly mean sea level data were obtained from the Permanent Service for Mean Sea Level (1977). All existing sea level data are collected in three volumes which include revised data from previous IAPSO publications. Data from Volume 2: North, Central, and South America are used in this study.

The SST data are on a tape obtained from the British Meteorological Office. This contains SST ship data from the TDF-11 deck at the National Weather Records Center in Asheville, N.C. and monthly mean 5^{o} quadrangle averages for the Northern Hemisphere, 0^{o}-80^{o}N, during the period 1854-1968.

The British Meteorological Office (1978) has recently published the following procedures used in the quality control of the SST data:

> The observations for the whole period of record are grouped according to the area and time of year. Averages and standard deviations are formed for each 1^{o} latitude/longitude area (square) and each of 73 five day periods (pentads). For each area the variations of the average and standard deviation through the year are smoothed using the first two harmonics for the average and the first four harmonics for the standard deviation. The smoothed data are then combined to form long period averages for each 5^{o} square and each pseudo-month (a period of 6 pentads, 7 in August). The pentad 1^{o} square means are expressed as fractions of the monthly 5^{o} square

mean and these are stored for later use (A). The variance of the pentad 1^{o} square means about the monthly 5^{o} square mean is evaluated (B).

The observations for an individual year are grouped according to 1^{o} square and pentad. The mean for each group is multiplied by the fraction at (A) above in order to produce a value which is representative of the mid-month and mid-point of the 5^{o} square. The mean and variance of those values which relate to an individual 5^{o} square and pseudo-month (150 values, 175 in August) are then evaluated. The mean is tested against the 1% confidence limits of the distribution of values in different years. The variance is compared, using Snedecor's F test, with the variance indicated by the previous analysis covering the whole period of record (B). This test identifies distributions in which the mean may have been affected by an abnormally high proportion of outlying values. Approximately 10% of means or variances fail one or other of these two tests; in either case the mean is replaced by a value interpolated from the two preceding and two following months.

For each 5^{o} square a 12 column matrix is formed from the array of monthly mean values and an eigenvector analysis is performed. This separates the variation over the year into 12 orthogonal components, some of which are real variation and some spurious. As sea surface temperature anomalies change only slowly from one month to the next, only those eigenvectors together usually account for over 90% of the total variance. Finally, the data are reconstituted from the products of the eigenvectors representing real variation and their respective annual coefficients.

It is important to note that since the SST data have been smoothed, the magnitude of any SST anomaly patterns can be expected to be less than if original unsmoothed data were used.

The 700 mb temperature data are from an NCAR tape of winter mean 700 temperatures, 1947-1977 on a 5^{o} grid. The 300 mb geostrophic winds were computed by an NCAR library subroutine which utilizes the NCAR tape of monthly mean 300 mb heights during the period 1963-1977 on a 5^{o} grid interpolated from the original NCAR 47 x 51 octagonal northern hemispheric grid.

Chapter 3

THE GREENLAND SEESAW DEFINED

Ever since European explorers, missionaries, and settlers have lived in Greenland and had contact with relatives and friends in Europe, they have noticed an interesting phenomenon: in a surprisingly large number of winters either Greenland has a relatively severe winter when Europe has a relatively mild one, or vice versa. This relationship has been investigated by various researchers including Dove, Hann, Walker and Bliss (as part of their North Atlantic Oscillation), Ångström, and Loewe (see literature review in van Loon and Rogers, 1978).

The most recent treatment of the Greenland seesaw is by van Loon and Rogers (1978) (hereafter referred to as vLR), and it is their definition of the seesaw which provides the point of departure for this study. They define the seesaw in terms of long term temperature records from Jakobshavn in Greenland and Oslo in northwestern Europe. The criteria for defining a seesaw winter are that the difference in departures from the respective means of the two stations be greater than or equal to $4^{o}C$ and opposite in sign. The magnitude of the threshold difference is designed to be sufficiently large to filter out noise and give clearer pressure anomaly patterns.

The two modes of the seesaw are GB: Greenland below normal and Europe above, and GA: Greenland above normal and Europe below. Using the $4^{o}C$ difference criterion, a list of GB and GA winters was derived and appears in Table 1. During the period of record, there

TABLE 1

WINTERS 1840-1977, MINUS 1852-1856, WHEN THE WHOLE SEASON WAS GA/GB OR BB/BA

WINTERS (DJF)			
Greenland Above	Greenland Below	Both Above	Both Below
1976-77	1972-73	1964-65	1969-70
1974-75	1971-72	1942-43	1967-68
1968-69	1970-71	1934-35	1953-54
1962-63	1948-49	1933-34	1896-97
1958-59	1936-37	1932-33	1867-68
1947-48	1924-25	1931-32	1848-49
1946-47	1920-21	1930-31	1844-45
1941-42	1914-15	1929-30	1843-44
1940-41	1913-14	1926-27	
1939-40	1910-11	1912-13	
1928-29	1909-10	1872-73	
1927-28	1908-09	1871-72	
1925-26	1906-07	1850-51	
1894-95	1905-06	1842-43	
1892-93	1898-99		
1880-81	1987-98		
1878-79	1895-96		
1876-77	1893-94		
1874-75	1889-90		
1870-71	1886-87		
1869-70	1883-84		
1860-61	1881-82		
1859-60	1873-74		
1846-47	1865-66		
1840-41	1863-64		
	1862-63		
	1858-59		
	1857-58		
	1841-42		
25	29	14	8

were 25 GA winters and 29 GB winters giving a total of 54 seesaw winters and a 40.6% occurrence rate. As vLR point out, if winter months are considered on an individual basis, there is a higher rate of occurrence. However, the 4^{o} criterion becomes more stringent when applied to a three month average. Therefore, winter averages (December, January, and February) were used to provide further filtering to eliminate as much noise as possible and give clearer anomaly patterns.

Figure 1 (after vLR) depicts the January mean temperature difference, GB minus GA for stations with complete records since 1899. Much the same pattern exists for the winter temperature difference. There is the expected opposition of sign between Greenland and northern Europe, but it is interesting to note that an in-phase/out-of-phase pattern appears to set up around the Northern Hemisphere with the eastern U.S. out of phase with Greenland; the western U.S., southern Mediterranean, Middle East and North Africa are in phase with Greenland. The winter sea level pressure anomaly difference for GB minus GA appears in Figure 2. The sign of the anomaly resembles the GB mode. There is a large negative anomaly in the area of the Icelandic Low, a positive anomaly near the Aleutian Low, and positive anomalies stretching into the regions of the subtropical highs in both the Atlantic and Pacific. As vLR note, the pressure anomaly pattern in Figure 2 is very similar to the first eigenvector of January sea level pressure from Kutzbach's (1970) analysis which explains why the seesaw pattern has such a high rate of occurrence. The larger numbers in Figure 2 are pressure anomaly differences for individual stations with records prior to 1899. Record length for

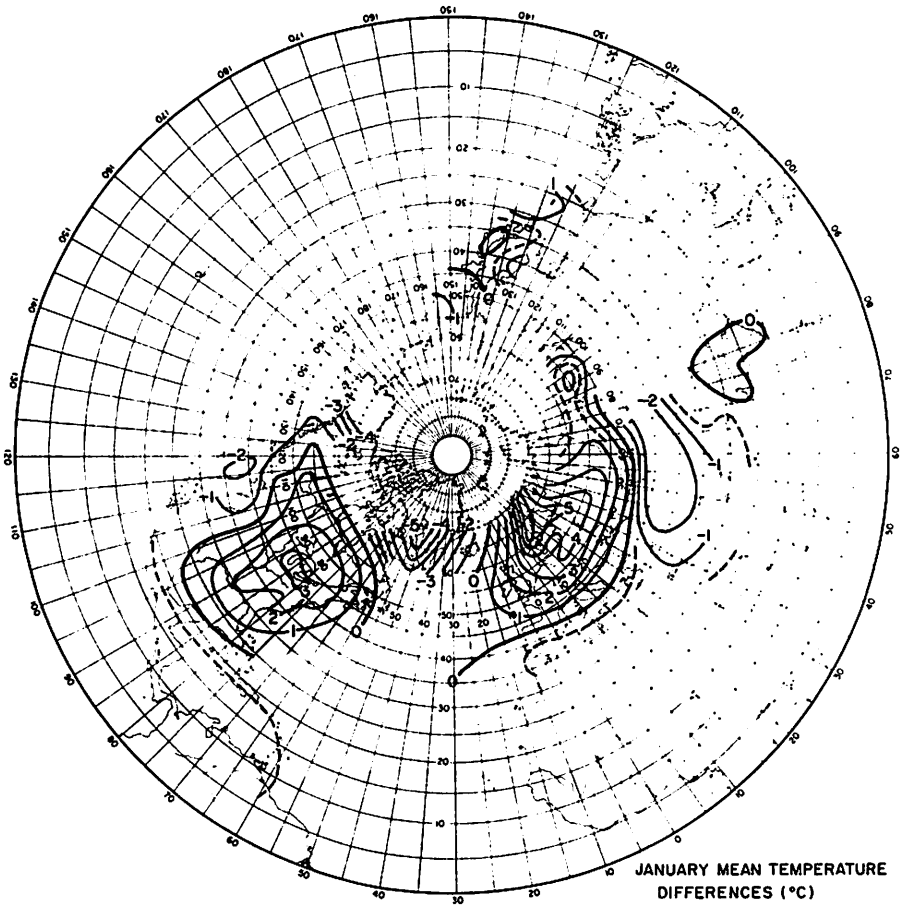

Figure 1. January mean temperature differences (°C) (after van Loon and Rogers, 1978).

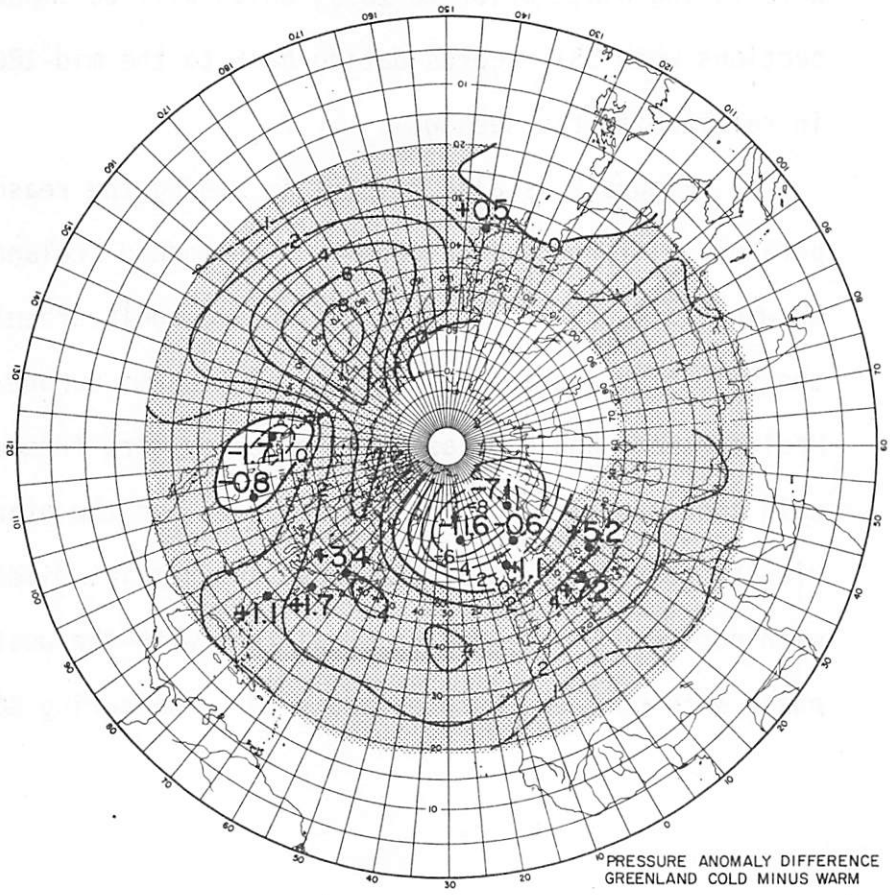

Figure 2. Sea level pressure anomaly difference, GB minus GA (mb).

North American stations goes back to around 1873, and for European stations to about 1840. It can be seen that in both sign and magnitude the pre-1899 pressure anomaly differences fit the post-1899 pattern very well. This indicates that the same seesaw processes were taking place prior to 1899, which will be important in later sections when SST records dating back to the mid-1800's are studied in relation to the seesaw.

Figure 2 is also helpful in seeing the reason for the temperature difference in Figure 1. A deepened Icelandic Low in the GB winters increases northerly flow and cools Greenland, while at the same time increased southerly flow warms Europe. The southern Mediterranean and Mid East are cooled by more frequent outbreaks of cold continental air. The eastern U.S., on the other hand, experiences fewer cold polar outbreaks and remains mild and in phase with northern Europe during GB winters with the western U.S. out of phase with northern Europe, and vice versa during GB winters.

Chapter 4

LITERATURE REVIEW AND HYPOTHESIS DEVELOPMENT

The trade winds seem to be a suitable starting point to review tropical teleconnections to midlatitude circulation since they have a direct relationship to several other parameters and are symptomatic themselves of a number of important processes. The role the trades play in determining SST's in the tropics has been discussed by Bunker (1976) and Bunker and Worthington (1976). They took into account trade wind strength as a factor in the bulk aerodynamic equations which determine heat transfer processes between air and sea and, ultimately, SST's themselves. Barnett (1977), McCreary (1976), Flohn and Fleer (1975), Wyrtki (1974), and Doberitz (1969) emphasized the close coupling between the trades and the tropical oceans. Davis (1976) pointed out that on time scales of one month to one year the atmosphere most likely drives the ocean. A number of investigators have established that trade wind intensity is closely linked to ocean upwelling and associated SST patterns (Hastenrath, 1977; Emery, 1976; Brown, 1963). Similarly, changes in trade wind strength and the resulting tropical SST variations have been pointed to by Bjerknes (1966, 1969) and later by Pittock (1973) and Reiter (1978a) as the starting point for a chain of events which ultimately influences midlatitude weather.

Tropical SST's and their possible relationships to midlatitude weather have also been considered on their own account without causative link to trade wind variations. The position and

nature of the tropical SST maximum have been recognized as being important to regional and global circulation patterns and processes (Hastenrath and Lamb, 1977a and b; Lamb, 1977; Ramage, 1977, 1974; Kidson, et al., 1969). Haworth (1978) established a strong connection between tropical SST's and midlatitude pressure patterns.

Another vital trade wind-related parameter in the tropics whose influence spreads to extra-tropical latitudes are wind-driven ocean currents. These have been recognized as being important in the advection of warm water that influences weather not only within the tropics (Wyrtki, 1975, 1974, 1973; Namias, 1973; Hickey, 1975) but in midlatitudes as well (Reiter, 1978a and b; Bjerknes, 1960; Brooks, 1931). Reiter details how increased trade wind strength increases current speeds and advection rates around the whole Pacific gyre which eventually warms midlatitude SST's and affects weather around the Northern Hemisphere. The concept of trade wind intensity indirectly altering midlatitude SST's through ocean current advection is of great interest since a number of researchers have linked northern ocean SST anomalies to variations in hemispheric weather patterns (Namias, 1978, 1975, 1972, 1969, 1964, 1959; Ratcliffe and Murray, 1970; Sawyer, 1965).

With the increased sophistication of general circulation models in recent years, a number of studies have been done to try and assess the influences of SST anomalies on weather, and, in particular, to what degree tropical SST anomalies affect global circulation patterns. Rowntree (1972, 1976a and b) in a series of experiments using both hemispheric and global general circulation models found that SST anomalies in the tropics produced widespread

global circulation changes. However, other numerical experiments have produced somewhat contradictory results. Washington and Chervin (1977) showed that altering Indian Ocean SST's in the NCAR general circulation model (GCM) produced mostly local effects. Again using the NCAR GCM, Houghton et al. (1974) and Chervin et al. (1976) prescribed large midlatitude SST anomalies, which, as seen previously, could possibly be the end result of tropical forcing. In both experiments the results were inconclusive with most circulation changes occurring in the immediate regions of the anomalies. However, both studies agreed that important downstream teleconnections could exist but were unclear due to the nature of the difficulties involved with the numerical model used. Ramage (1977) addresses these difficulties and points to the need for better parameterizations of the physical processes involved in air-sea interaction.

In a slightly different vein, experiments performed by Salmon and Hendershott (1976) using a simple atmospheric model linked to a simple ocean model suggest that SST anomalies are the result of atmospheric pressure anomalies on time scales of less than one year. This would seem to indicate that on short time scales, the atmosphere does not respond significantly to SST variations. In the words of Salmon and Hendershott, the atmosphere is "too noisy" to be affected by SST anomalies on time scales of less than one year.

However, the results of a recent experiment conducted by Julian and Chervin (1978) seem to agree with the earlier hypotheses of Bjerknes, Rowntree and others that tropical SST's are very closely associated with midlatitude circulation. Using the NCAR GCM, Julian and Chervin found that eastern Pacific SST's are closely linked to

the strength of the westerlies, on seasonal time scales, and that atmospheric circulation is probably more sensitive to changes in tropical SST's than to changes in midlatitude SST's.

Another important tropical parameter to be considered is rainfall. Since maximum values of tropical precipitation are generally associated with upward motion in the Intertropical Convergence Zone (ITCZ) (Griffiths, 1972), variations in the excursion of the ITCZ and resulting deficiencies in precipitation have been identified as being responsible for major tropical droughts in South America and Africa (Lamb, 1978; Kraus, 1977a; Hastenrath, 1976; Tanaka et al, 1975; Riehl, 1973). Migration of the ITCZ is obviously important in the tropics, but it has also been suggested that the position of the ITCZ is a function of the cross-equatorial energy flux and transport of energy to higher latitudes (Kraus, 1977a and b; Newell et. al., 1974). Excursion of the ITCZ, as defined by the area of highest rainfall, could, therefore, play a vital role in determining midlatitude atmospheric circulation.

The position of the subtropical jet is thought to mark the poleward edge of the equatorial Hadley cell (Palmén and Newton, 1969). The subtropical jet, as defined by the upper tropospheric west wind maximum, is also considered to be a manifestation of tropical westerly momentum transfer to the midlatitudes (Krishnamurti, 1961). Latitudinal position, therefore, is very important in terms of extent of the Hadley circulation and the magnitude of westerly momentum being infused into the midlatitudes from the tropics (Weinert, 1968; Bjerknes, 1966).

A final consideration that could shed some light on tropical-midlatitude interactions is the reaction of a number of different processes at various locations in seasons prior to and after seesaw winters. Case studies have been conducted to try and ascertain what events in various latitudes in preceding seasons lead up to an anomalous circulation event (Namias, 1978; Reiter, 1978; Krueger and Winston, 1975; Bjerknes, 1969; Bjerknes, 1966). It is obvious that if indications of a forthcoming midlatitude circulation anomaly could be documented, say, in the tropics (if the tropics "lead" the mid-latitudes), then this could have important forecast value.

From the preceding ideas presented in the literature, it is now possible to formulate the following working hypothesis which will be tested and either confirmed or amended in the course of the following investigation. For GB winters (vice versa for GA winters): An expanded and strengthened Hadley cell in the Northern (winter) Hemisphere is associated with stronger trades which lower SST's in the tropics and intensify ocean current circulations. In conjunction with the vigorous Hadley cell, there is a southward excursion of the ITCZ, a northward shift of the sub-tropical jet, and strengthened midlatitude westerlies.

Chapter 5

TRADE WIND SYSTEMS

Since the pressure anomaly patterns of the midlatitude seesaw winters shed significant light on defining seesaw circulation processes, it seems reasonable to begin with pressure relationships in the tropics to see in just what ways the midlatitudes and the tropics are tied together during seesaw winters. The correlation of sea level pressure between the key point 70^{o}N, 20^{o}W and all other points on the 5^{o} grid for 26 seesaw winters appears in Figure 3. The key point was chosen because it coincided with the largest pressure anomaly difference in Figure 2. The most obvious feature of Figure 3 is that the northern regions are out of phase with the subtropical areas of the Northern Hemisphere. Most notably the Icelandic Low is out of phase with the Atlantic and Pacific subtropical highs, which would imply that a deepening Icelandic Low would be accompanied by a building of high pressure in the subtropics and vice versa. This relationship is apparent in Figure 2, where positive pressure anomalies in the subtropics occur with negative anomalies in the Icelandic Low region in the GB winters, vice versa for the GA winters. This strengthening and weakening of the subtropical high pressure belt between GB and GA winters are very important because the stronger the subtropical high, the stronger are the trade winds driven by it (Pittock, 1973). Similarly, the deeper the Icelandic Low, the stronger are the westerlies driven by it.

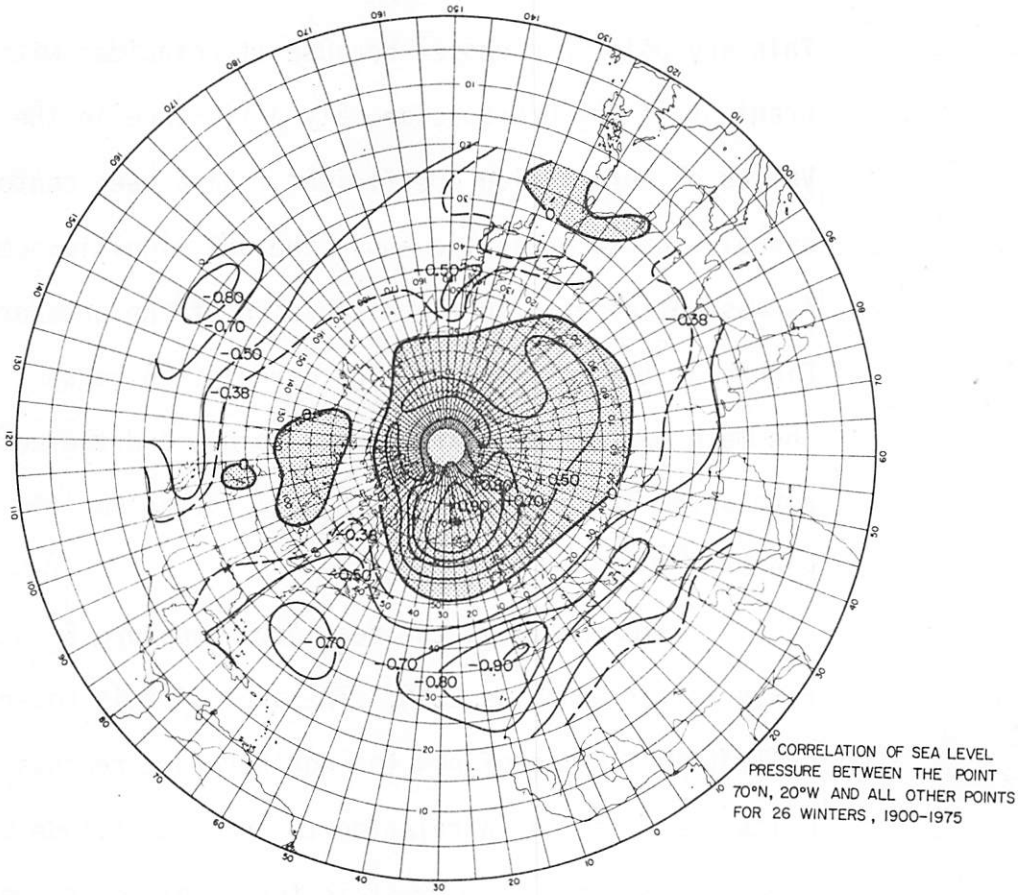

Figure 3. Correlation of sea level pressure between the point 70°N, 20°W and all other points north of 20°N for 26 winters, 1900-1975; shaded areas indicate positive correlations.

To explore the relation of midlatitude westerlies and tropical trade winds further, the zonal component of the geostrophic wind at the key point 52.5°N, 25°W was correlated with the numerical value of the zonal geostrophic wind at 5° grid points throughout the rest of the Northern Hemisphere for 26 seesaw winters (see Fig. 4). This key point was chosen because it coincided with the strongest gradient of the pressure anomaly difference in the westerlies. Values of correlation coefficient r have been contoured in Figure 4, and all shaded areas lie above the 95% significance level at r = 0.38. As was anticipated in the discussion of the pressure correlations in Figure 3, there is a very high correlation between the strength of the mean westerlies near the key point, and the northeast trade winds across the Atlantic and near Hawaii in the Pacific during seesaw winters.

Unfortunately, the sea level pressure 5° NCAR grids only reach as far south as 20°N. The area of this coverage gives an excellent indication of how the northernmost reaches of the trade wind belts are behaving in relation to the midlatitude westerlies but it remains a mystery as to what is taking place between 20°N and the equator, as well as what is going on in the region of the southeast trades south of the equator. Therefore it becomes necessary to choose various station pairs which straddle pressure gradients of interest. The variations in the sea level pressure differences between pairs of stations give an indication of the fluctuation of the calculated geostrophic wind speeds blowing perpendicular to the interval between the respective pairs. When computing geostrophic wind speeds very close to the equator, it has been pointed out that the

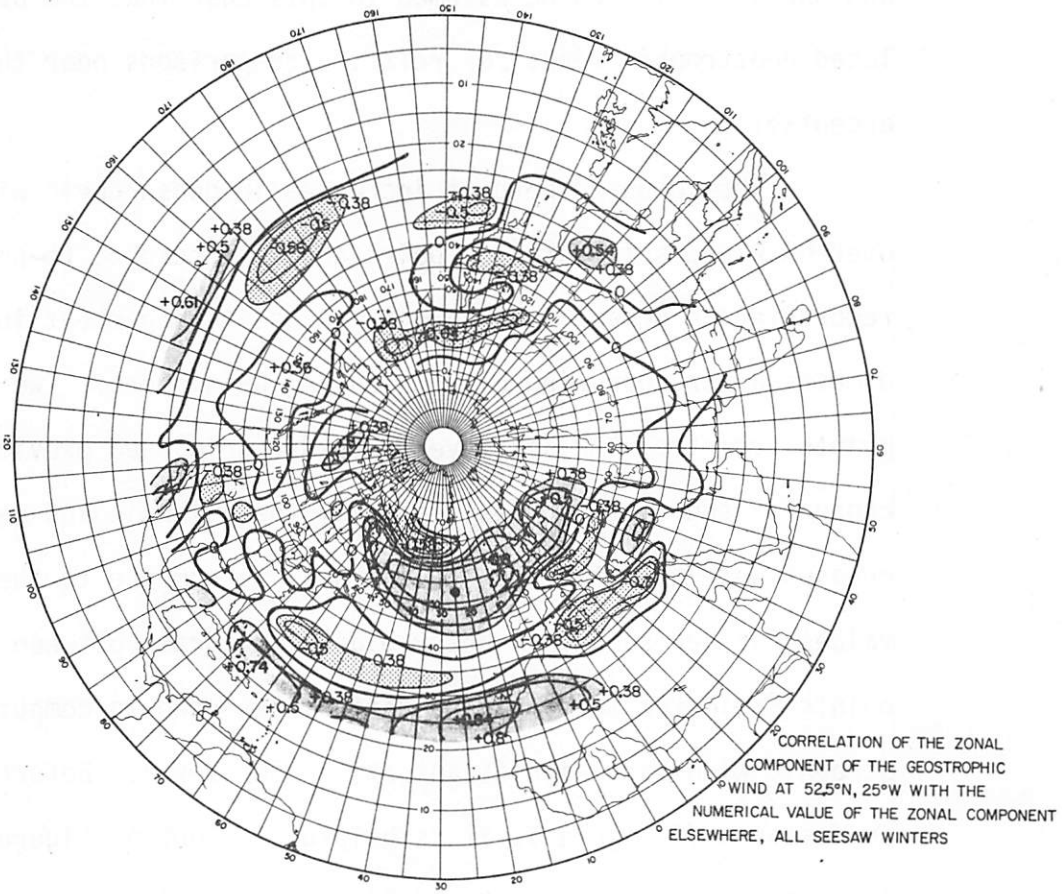

Figure 4. Correlation of the zonal component of the geostrophic wind at 52.5°N, 25°W with the numerical value of the zonal component elsewhere for all seesaw winters; shaded areas are above the 95% significance level (after Rogers and van Loon, 1978).

geostrophic approximation begins to lose credibility due to the negligible Coriolis force (Holton, 1972). However for the purpose at hand, a relative measure of trade wind intensity as indicated by pressure gradient fluctuations between GB and GA winters is desired, and therefore it can be assumed in this case that the use of calculated geostrophic winds for relative comparisons near the equator is acceptable.

The computed percent increases in geostrophic wind in GB over GA winters for station pairs chosen according to position and record length appear in Figure 5. A positive percent increase indicates a stronger wind blowing during GB winters. Two pairs of points from the NCAR sea level pressure grid used previously were chosen at the east and west edges of the Atlantic and percent increases were computed for them as well to compare to the station pair values further south. A heavy black line drawn between a pair of points indicates the pressure differences used to compute the geostrophic winds are significant at the 95% level. Before commenting on features of Figure 5, it is helpful to look at Figure 6 which illustrates the number of GB and GA winters available to compute the pressure differences in Figure 5. All pairs ringing the subtropical highs in the North and South Atlantic are fairly well represented, with the three pairs of high significance (dark axis line) coinciding with the pairs with the greatest degrees of freedom. The pairs from the Pacific are very weakly represented, but are included to give some indication of what could be taking place in that area. Other station pairs are fairly well represented, and should be reasonably reliable indicators of geostrophic wind strengths. Returning to

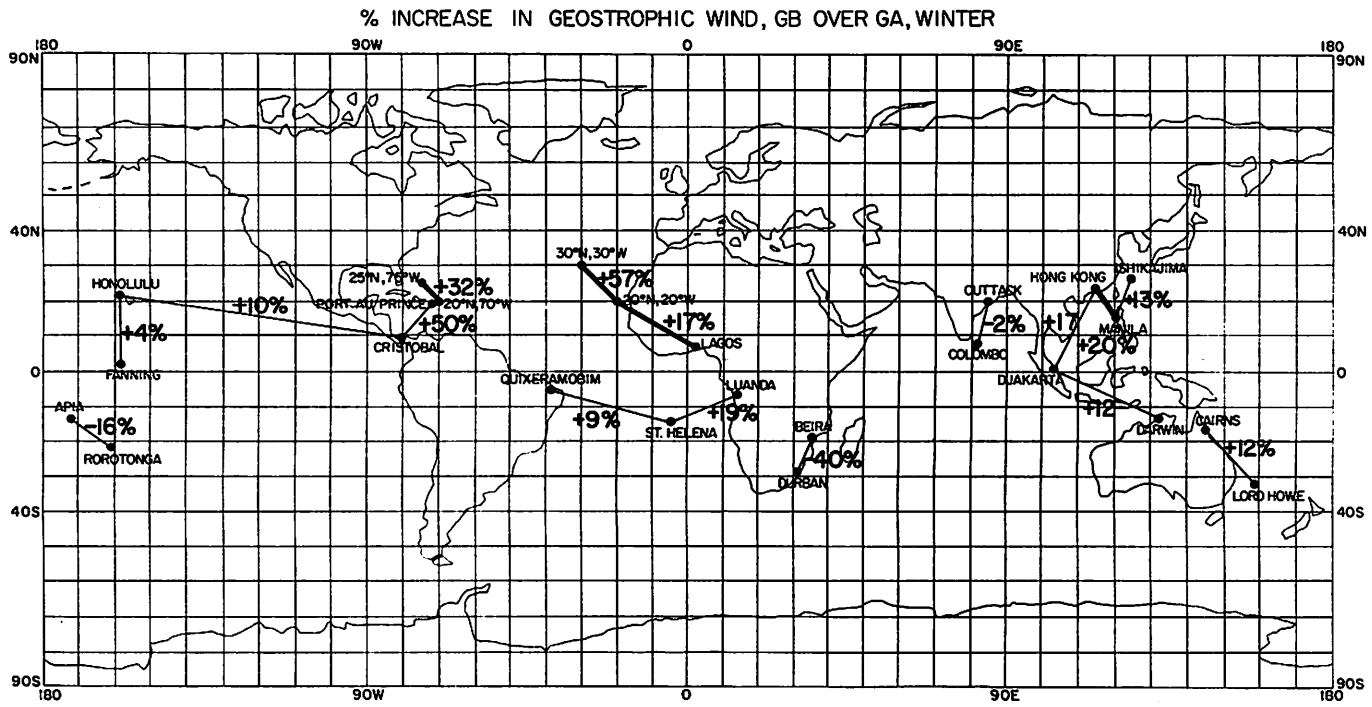

Figure 5. Percent increase in geostrophic wind normal to axis of station pair, GB over GA, winters.

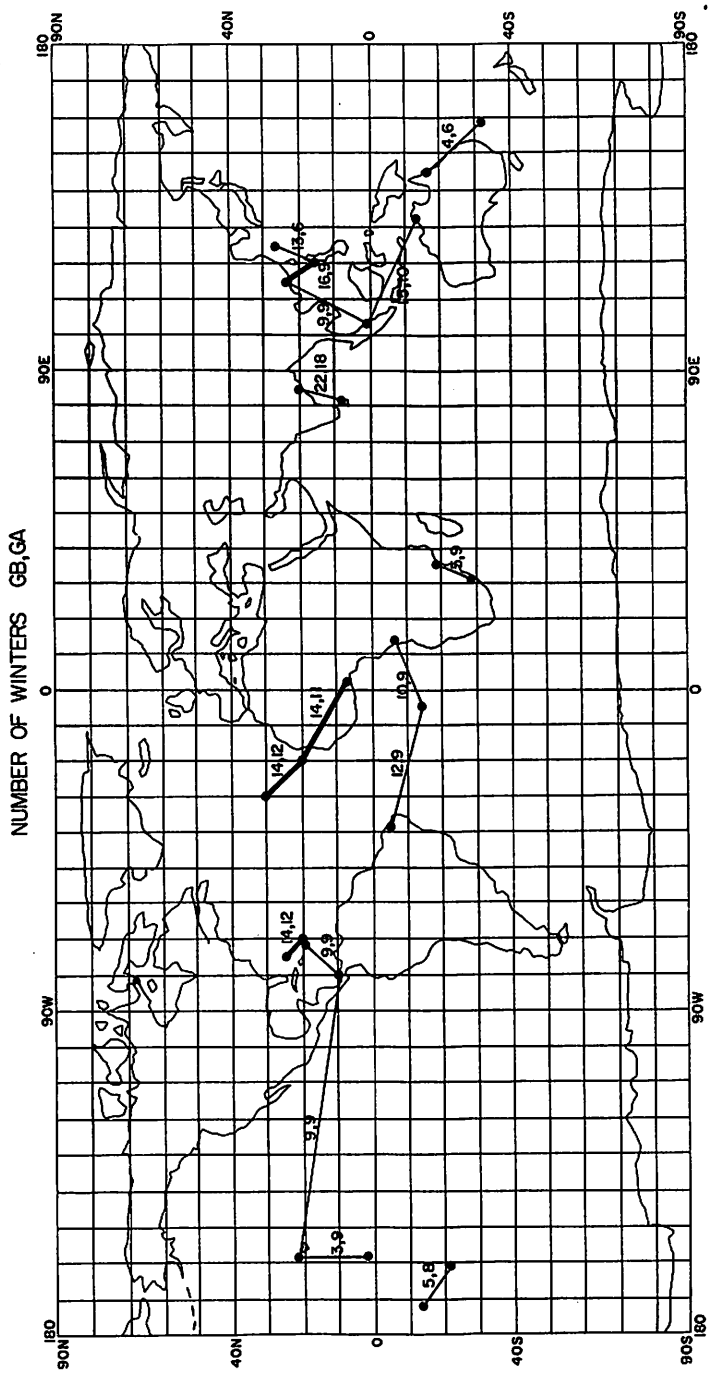

Figure 6. Number of GB and GA winters available for analysis at each station pair.

Figure 5, it is interesting to note that in almost all station pairs there is a positive percent increase indicating stronger trade wind flow in the GB winters, and weaker flow in the GA winters.

Starting with the Atlantic, there are stronger trade winds in the GB in all sectors. These pairs were chosen from the few available stations with sufficient record length that straddle the equatorial reaches of the subtropical highs. It was seen earlier in Figure 4 that an increase in westerlies in GB winters was accompanied by a similar increase of northeast trades in the 20-30^{o}N zone, and vice versa for GA winters. This result is verified by the present method used to compute the large significant increases seen at 25^{o}N, 75^{o}W -- 20^{o}N, 70^{o}W and 30^{o}N, 30^{o}W -- 20^{o}N, 20^{o}W. It is also apparent from Figure 5 that a similar relationship exists south of 20^{o}N as indicated by the positive percent increases at Port au Prince-Cristobal in the Caribbean and 20^{o}N, 20^{o}W -- Lagos in the eastern Atlantic sector. In the North Pacific, positive percent increases are seen between Honolulu-Cristobal and Honolulu-Fanning. Thus, stronger westerlies and stronger tropical Atlantic easterlies seem to be linked with stronger northeast trades in the North Pacific. A similar link seems to exist in the southeast Asian-Indonesian area.

This in-phase relationship appears to be the case in the South Atlantic as well. Both pairs in this area are indicators of southeast trade wind strength and undergo intensified flow in GB winters in a similar sense to the Northeast trades in the North Atlantic and North Pacific.

To explore the interrelationship between northeast and southeast trades in the Atlantic further, correlations were computed for

the pairs 20^{o}N, 20^{o}W -- 30^{o}N, 30^{o}W and Luanda-St. Helena (Table 2). They were chosen as representative indicators of the intensities of the northeast and southeast trade winds, respectively. It can be seen in Table 2 that in 57 winters common to both, the correlation coefficient between the two pairs is $r = 0.34$ which is significant at the 95% level. However, taking only the 19 seesaw winters common to both pairs, the correlation coefficient jumps to $r = 0.64$, which is significant at the 99% level. Excluding seesaw winters from the whole series (leaving 38 winters), the correlation coefficient drops to $r = 0.28$ which is below the 95% significance level. Therefore, assuming that these two pairs of data points are representative of Atlantic trade wind activity, it would appear that in all winters the northeast trades and southeast trades in the Atlantic are well correlated, very highly correlated during seesaw winters, and weakly correlated in non-seesaw winters.

TABLE 2

CORRELATION OF NORTHEAST AND SOUTHEAST TRADES
($20^{o}W$, $20^{o}N$-$30^{o}W$, $30^{o}N$; Luanda-St. Helena)

Winters common to both pairs	Correlation coefficient r	Degrees of freedom	Significance
All winters	0.34	57	95%
Seesaw winters only	0.64	19	99%
Non-seesaw winters only	0.28	38	---

Chapter 6

AFRICAN PRECIPITATION

Position of the ITCZ has been mentioned previously as being important in terms of cross equatorial fluxes of energy from the tropics to higher latitudes in the winter hemisphere (Kraus, 1977a; Newell et al., 1974). It is, therefore, of interest to see if any shifts of the ITCZ, as defined by the belt of maximum precipitation, can be discerned between seesaw modes.

In this analysis it should be noted that seesaw Januaries are used instead of seesaw winters for two reasons. First, the furthest southward excursion of the ITCZ in Africa usually occurs during January (Griffiths, 1972). Second, a comparison to another mode of circulation (the BB and BA modes of the seesaw as defined by vLR) is made possible by using Januaries since BB and BA winters during the period of record are very infrequent compared to single BB and BA Januaries. See Table 3 for a list of seesaw Januaries.

A GB or GA seesaw January is derived in the same manner as a seesaw winter using the $4^{o}C$ criterion described earlier. The two other patterns defined by vLR are used here for comparison: BB - both Jakobshavn in Greenland and Oslo in northwestern Europe have Januaries with below normal temperatures, and BA - both Jakobshavn and Oslo have Januaries with above normal temperatures. The criterion is that both stations must have temperature departures of at least $1^{o}C$ above or below their respective long term January means. The BB and BA winters listed in Table 1 were derived in a similar manner except that winter means were used instead of January means.

TABLE 3

SEESAW JANUARIES

GB	GA	BA	BB
1902	1912	1916	1899
1904	1917	1926	1901
1905	1929	1927	1914
1906	1931	1928	1918
1909	1940	1930	1922
1911	1941	1934	1950
1919	1942	1935	1956
1923	1943	1936	1966
1925	1945	1939	1968
1932	1948	1962	1970
1933	1953	1964	1972
1937	1954	1965	
1938	1959	1969	
1944	1963	1973	
1949	1975		
1971			
16	15	14	11

The heavy contour drawn across southern Africa between about 10^{o}S and 15^{o}S on Figure 7 encloses the area that, on the average, receives a January rainfall maximum in amounts greater than 200 mm (taken from Jackson, 1961). Elsewhere, January rainfall is below 200 mm. Rainfall records for stations in the region of this January rainfall maximum were analyzed and the differences are shown in Figure 7 between GB minus GA Januaries (a) and BA minus BB Januaries (b). The main difficulty encountered in this analysis was the short period of record of a number of the stations. An indication of data coverage can be gained in Figure 7c and d which illustrates the number of Januaries in each mode available for analysis. Due to the dearth of historical data, as well as the high variance of the rainfall records, the standard two-tailed t test for significance of the differences in Figure 7 is not very effective. However, a very interesting pattern emerges from looking at the sign of the differences in Figure 7a. The stippled area indicates a band of stations south of the long term January precipitation maximum with positive deviations indicating greater precipitation during GB Januaries. Stations north of about 9^{o}S cannot be considered here due to the fact that those stations are in the area of a double rainfall maximum (Griffiths, 1972). However, within the outlined January precipitation maximum there are mostly negative precipitation differences. This would seem to indicate that during GB Januaries the belt of maximum precipitation is shifted further south than during GA Januaries. Assuming that the rainfall maximum is associated with the position of the ITCZ (Griffiths, 1972), the ITCZ would appear to shift south during GB Januaries. To compare the GB minus GA

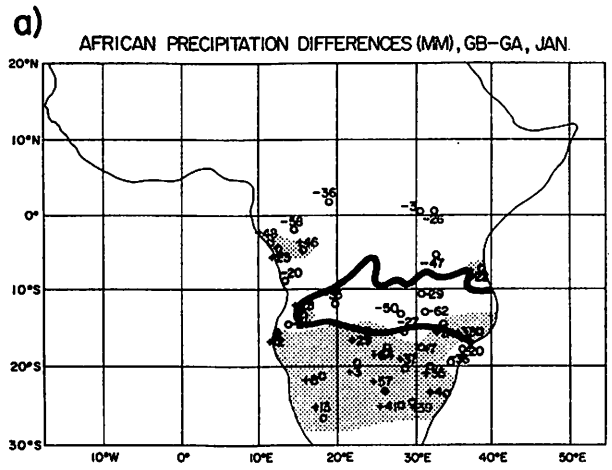

Figure 7.a Precipitation differences, GB minus GA for January, stippled areas indicate regions of positive differences. Dark contour outlines area of rainfall greater than 100 mm.

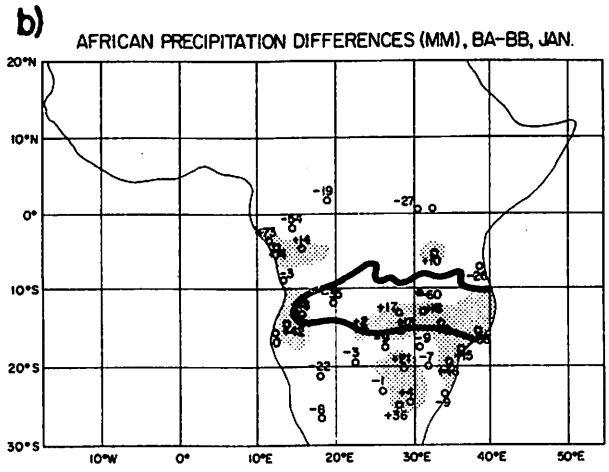

Figure 7.b Precipitation differences, BA minus BB, for January. Dark contour same as in part a.

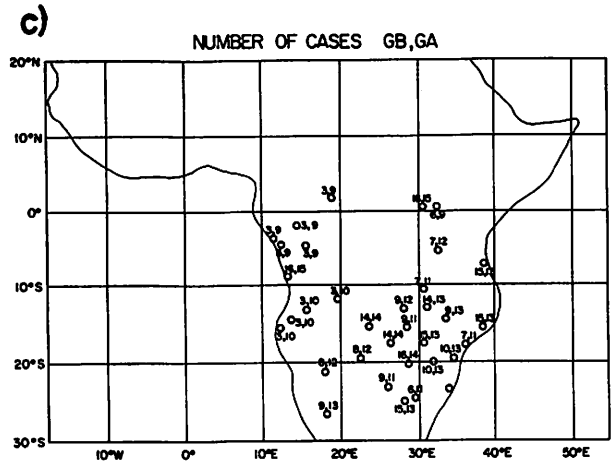

Figure 7.c Number of GB and GA Januaries available for analysis at each station in part a.

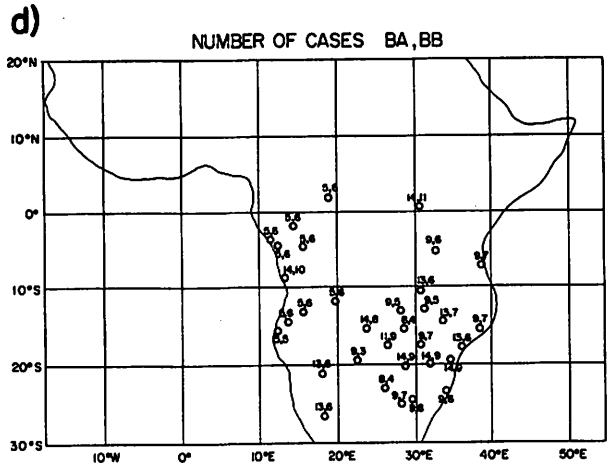

Figure 7.d Number of BA and BB Januaries available for analysis at each station in part b.

precipitation differences to another mode of seesaw circulation, refer to the BA minus BB precipitation differences in Figure 7b. The pattern lacks the coherent shift seen in Figure 7a.

The position of the ITCZ in January is shown in Figure 8. The east-west axis lies at about 15^{o}-18^{o}S. Referring back to Figure 7, the precipitation maximum defined by Jackson lies between 10^{o}S and 15^{o}S which is to the north of the ITCZ itself. Nieuwolt (1977) points out that the maximum precipitation usually occurs within the air mass which carries the most moisture and not necessarily at the location of the air mass discontinuity as defined by the ITCZ. This characteristic is evident here because the major moisture source for January rainfall in this region is the Congo air mass to the north of the ITCZ (Taljaard, 1972). Since transport of moisture over the African continent is thought to be primarily associated with the mean wind (Peixoto and Obasi, 1965; Flohn and Korff, 1965) then, as can be seen from the streamlines of surface wind in Figure 8, moisture is most likely being carried in from the tropical Atlantic by the southeast trades which then turn south toward the ITCZ. A secondary moisture source is the Indian Ocean east of Africa but, as Taljaard (1955) points out, the topography of Africa is such that most of the moisture from the Indian Ocean is rained out when the air is lifted near the east coast en route to the central plateau area. It follows that a chief control on most of the moisture transported into the area of the January precipitation maximum in Africa is the strength of the southeast trades off the west coast. It has already been seen that during GB winters the southeast trades tend to be more intense than during GA winters implying more vigorous

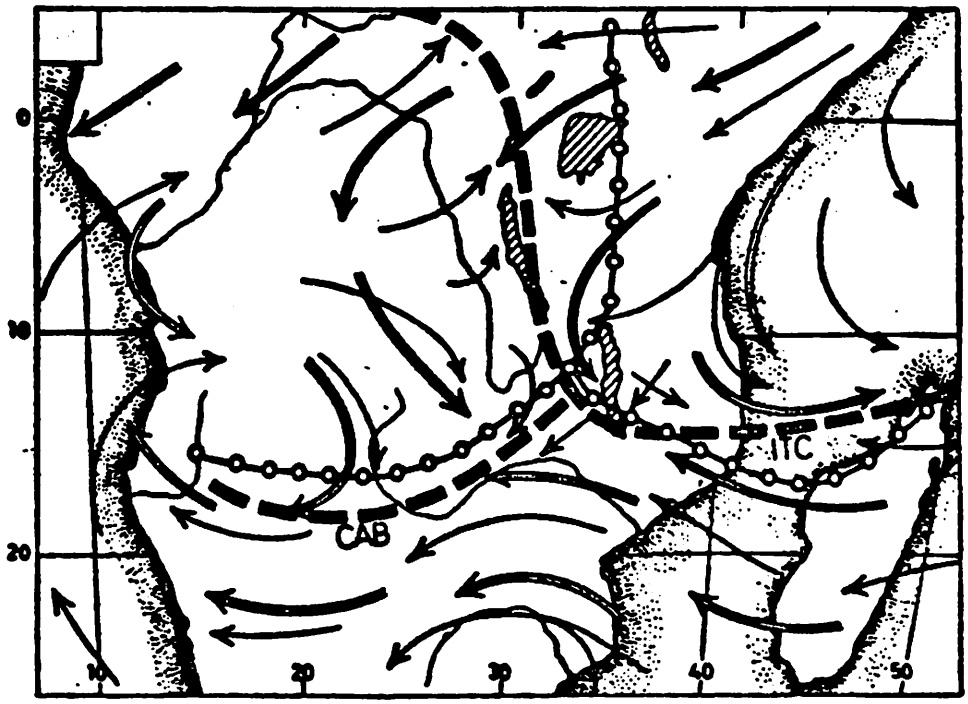

Figure 8. January mean low level circulation over southern Africa. Single lines indicate near surface flow, double lines indicate 3-km flow. Dashed lines indicate ITC and the Congo air boundary in January and February 1958. Linked circles are the troughs in the same months (after Taljaard, 1972.)

transport of moisture toward the ITCZ which is positioned further south.

Chapter 7

OCEANIC RESPONSES

Sea level fluctuations as indicators of Gulf Stream intensity

It was mentioned earlier that ocean current gyres may respond to variations in wind stress (e.g., Reiter, 1978). Therefore, since the Gulf Stream is an integral part of the Atlantic current gyre and transports large amounts of heat northward from the tropics to the midlatitudes, it is of interest to assess the response of the Gulf Stream to variations in trade wind strengths across the tropical Atlantic.

In the following analysis, relative sea levels from pairs of stations are used to give indications of changes in geostrophic surface current strength. This method has been used by a number of investigators in a variety of applications (e.g., Niiler and Richardson, 1973; van Loon, 1972; McKee, 1971; Montgomery, 1938). The general theory of why a sea level difference exists across an ocean current stems from the fact that a geostrophic balance must exist between the Coriolis force and the pressure gradient across the current as evidenced by a change in sea level. Niiler and Richardson (1973) give the following equation which relates the change of sea level, n_{oL}, across a distance L (between o and L), the velocity V_s of a current such as the Gulf Stream flowing perpendicular to the axis of o and L, and the Coriolis force f:

$$n_{oL} = \frac{f}{g} \int_{L_o}^{L} V_s(x)\, dx$$

where g is the acceleration of gravity. The quantity n_{oL} is the absolute change of sea level which can only be used if sea levels at o and L are measured from the same bench mark.

There are a number of important factors that influence relative sea levels which can obscure results extracted from a study of current speeds using difference in sea level. Among these are (1) changes in local atmospheric pressure; (2) changes in the heat content and thus density of the water by variations of solar radiation, wind cooling, or advection; (3) changes in water salinity; (4) Ekman divergence or convergence, and (5) "set up" of water caused by wind stress piling up water in one area (Hickey, 1975; Lisitzin and Pattullo, 1961; Pattullo, 1960; Pattullo et al., 1955; Montgomery, 1938). Of these, Lisitzin and Pattullo (1961) concluded that isostatic changes (water mass remains the same) of steric (density related) levels predominates sea level variations at low and subtropical latitudes, while in higher latitudes (greater than 40^{o}-45^{o}N) isostatic responses to changes in local atmospheric pressure are most important.

In this analysis, eight coastal stations stretching from Miami Beach to Atlantic City were paired with Bermuda to try and gauge the relative intensities of the Gulf Stream between modes of the seesaw. Since east coast stations and Bermuda do not have a common reference bench mark, only a relative measure of the geostrophic surface current is possible. It is safe to assume that all

pairs straddle the Gulf Stream because it has never been observed east of Bermuda (Stommel, 1960). Bermuda's sea level records date back only to 1932 (which is longer than any other recording location in the Caribbean) making it the only island station practicable for use in this analysis. In Figure 9, the relative difference of sea level in millimeters for each station, GB minus GA winters, is labeled on the axis of each pair for five GA winters and four GB winters. Generally, the greater the difference in sea level between two stations, the greater the relative velocity of the current flowing between the two stations (Niiler and Richardson, 1973). All station pairs chosen show negative differences, with the pairs Bermuda-Hampton Roads and Bermuda-Portsmouth significant above the 95% level. The negative differences indicate that a stronger gradient exists during GA winters implying that the Gulf Stream flows faster during those winters. Therefore, it appears that during the GB winters increased trade winds in the Atlantic are associated with decreased Gulf Stream velocities and vice versa for GA. This result would seem to contradict the theory of wind-driven ocean current circulation as treated by Munk (1950) and others which states that a circulatory current system, such as the North Atlantic, responds directly to the curl of the wind stress acting upon it. Bjerknes (1960) and Stommel (1951) even speak of intensification of the trades and westerlies having the effect of "speeding up" the North Atlantic gyre of which the Gulf Stream is a part. However, there is a degree of confusion in the literature concerning phase relations between ocean currents and winds in the Atlantic (Gill and Niiler, 1973; Kellerman, 1965; Niiler and Richardson, 1973; Stommel, 1960, 1953).

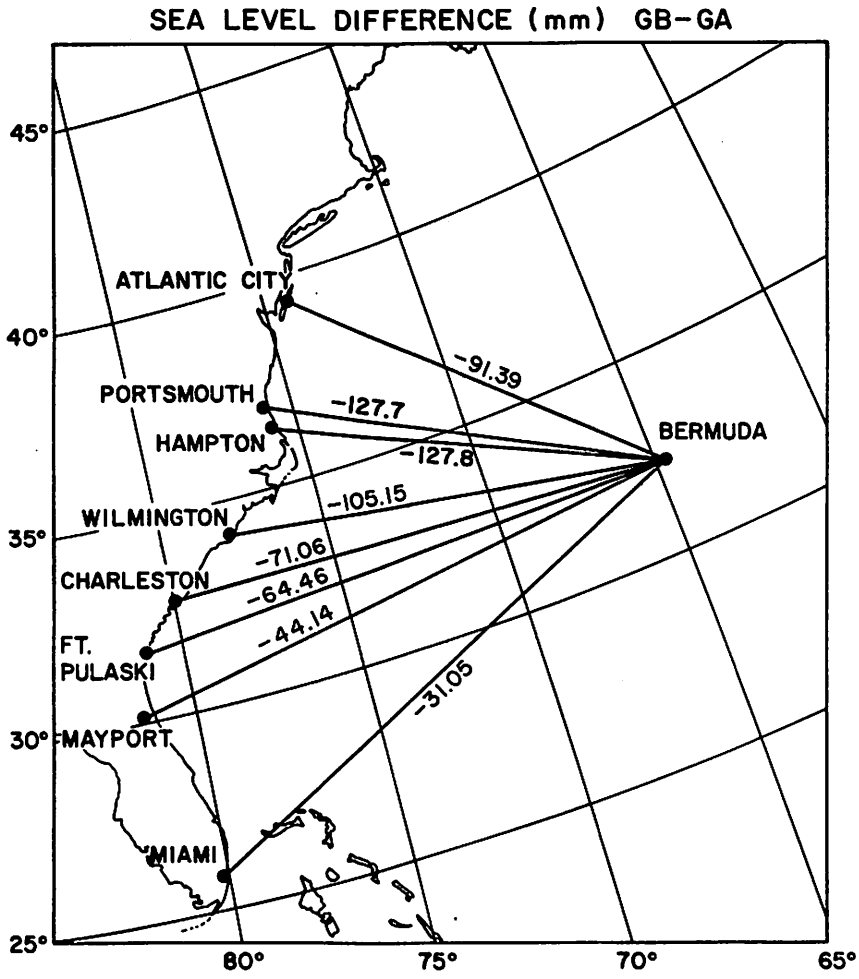

Figure 9. Relative sea level difference between Bermuda and east coast United States stations in mm. for nine GB minus GA winters.

There remains the possibility that the observed differences in sea level between Bermuda and the U.S. stations are due to some other, non-trade wind related process. It was mentioned earlier that steric effects and variations in air pressure are probably two of the most important factors in determining sea levels (Lisitzin and Pattullo, 1961). In a study involving sea levels in the Indian Ocean and South Pacific, Fairbridge and Krebs (1962) corrected sea levels for changes in sea level pressure (SLP). To check out the possibility that SLP variations determine the change of relative sea levels in this analysis, a correction factor of 1 cm change in sea level for each 1 mb change in atmospheric pressure was applied to the observed sea levels for each station (Lisitzin and Pattullo, 1961). SLP records were used either from the individual stations with both sea level and SLP records, or interpolated from nearby stations with SLP records (see Fig. 10). SLP anomalies used for the sea level corrections were computed by subtracting the respective winter departures from the annual means.

The corrected sea level differences appear in Figure 11. Comparing Figures 9 and 11, it can be seen that the corrected differences in Figure 11 are slightly smaller than the uncorrected ones in Figure 9, but the signs are still all negative which indicates stronger flow in GA and weaker flow in GB as before. This result seems to confirm Lisitzin and Pattullo's (1961) contention that variation of air pressure is not the most important consideration in determining sea levels at latitudes south of 40-45^{o}N. In the next section, steric influences will be examined in relation to the observed sea level variations.

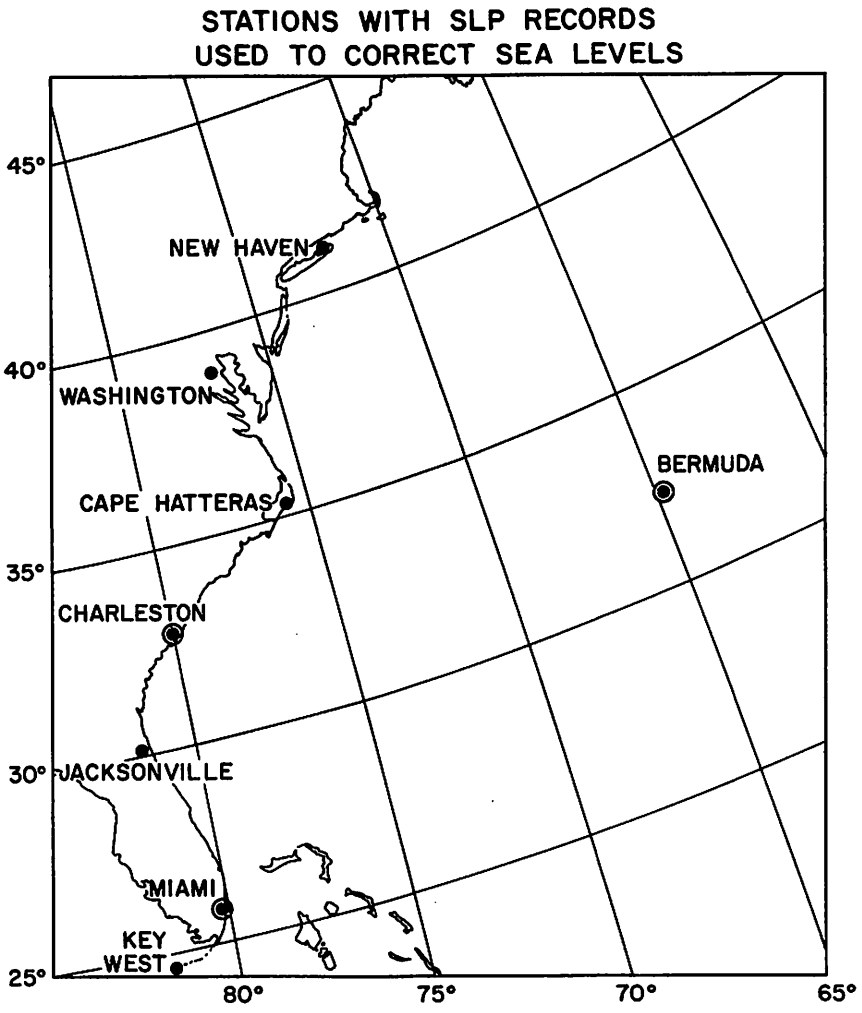

Figure 10. Stations with sea level pressure records used to correct recorded sea levels.

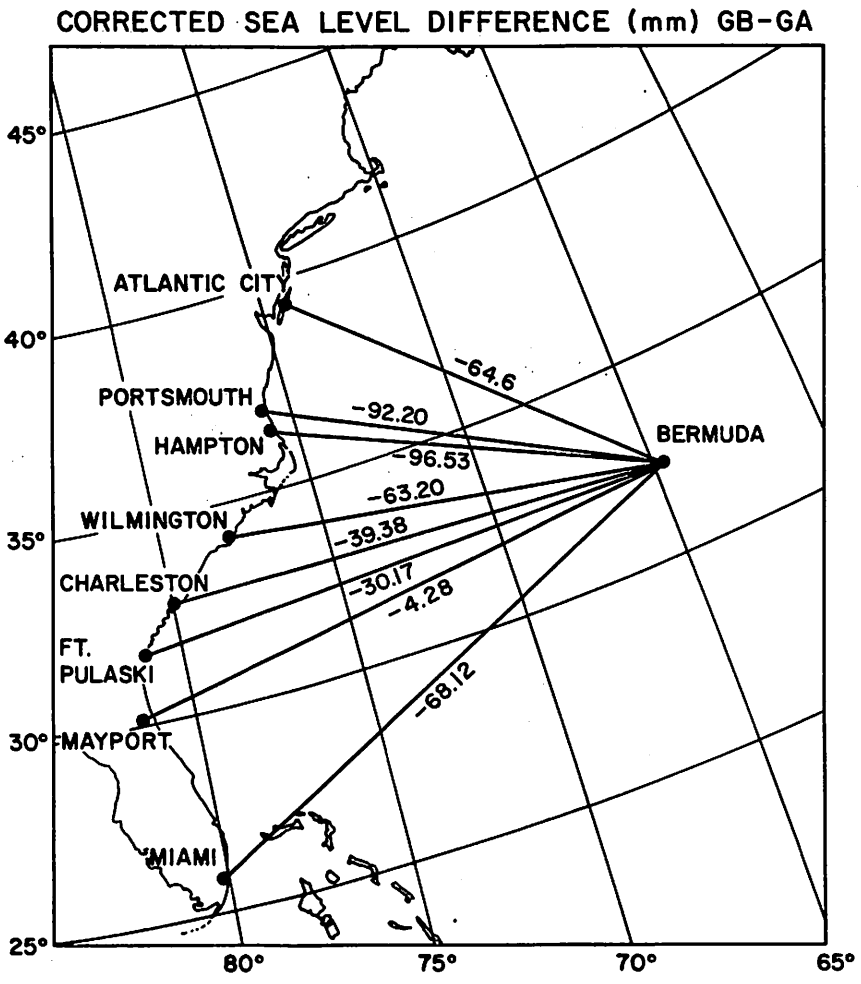

Figure 11. Sea level difference in mm. corrected for changes in sea level pressure for GB minus GA winters.

Sea surface temperature (SST) response

In the literature review earlier it was seen that many investigators have tried to link SST's and atmospheric circulation to clarify exactly what takes place in the complex set of processes that make up air-sea interaction. In this section, 5^{o} area averages of winter SST's are examined to see in what ways the surface temperature of the tropical oceans react during seesaw winters. The SST differences for GB minus GA winters during the period 1854-1968 in ^{o}C appear in Figure 12. Once again, the sign of the difference carries the sign of the GB winters. It is important to repeat at this point that (1) even though SST's analyzed here extend back to 1854, it was illustrated in Figure 2 that seesaw processes appear to be the same prior to 1899 when better Northern Hemisphere data coverage begins, and (2) the SST data are smoothed a great deal in the course of the quality control procedure described in an earlier section. Therefore, SST anomaly patterns can be expected to be of less magnitude than if original unsmoothed data had been used.

A number of interesting features are evident in Figure 12. First, an area of negative SST differences (colder water in GB, warmer in GA) covers the Atlantic between about $10^{o}N$ and $35^{o}N$. These differences are statistically significant as can be seen by referring to Figure 13. Positive differences exist in the Gulf of Mexico, in a small area off the Georgia coast, and in a strip stretching across the northern Atlantic near $40^{o}N$. Another positive area lies between 5^{o} and $10^{o}N$ and 33^{o}-$45^{o}W$. In the Pacific, a band of negative differences reaches almost all the way across the tropical regions south of $25^{o}N$ with the exception of an area of positive differences in the

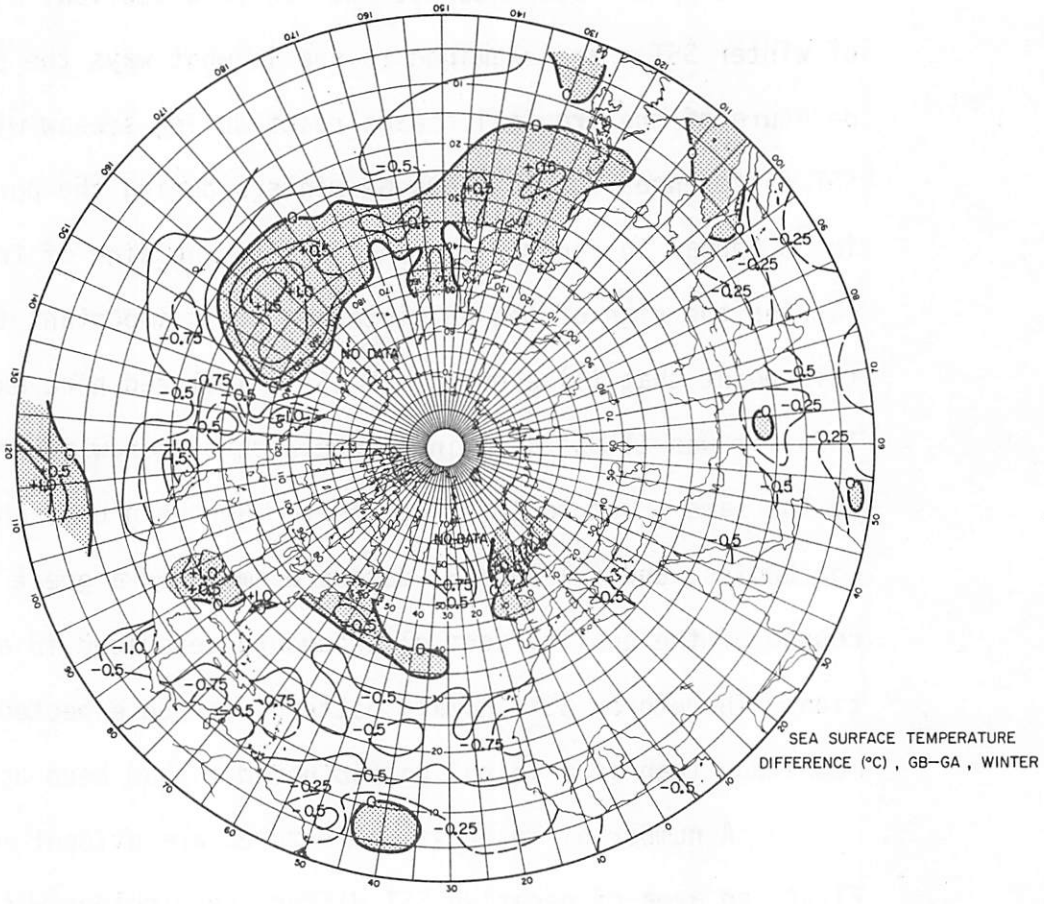

Figure 12. Sea surface temperature difference in ^{o}C for GB minus GA winters from 1854-1968. Positive differences are stippled.

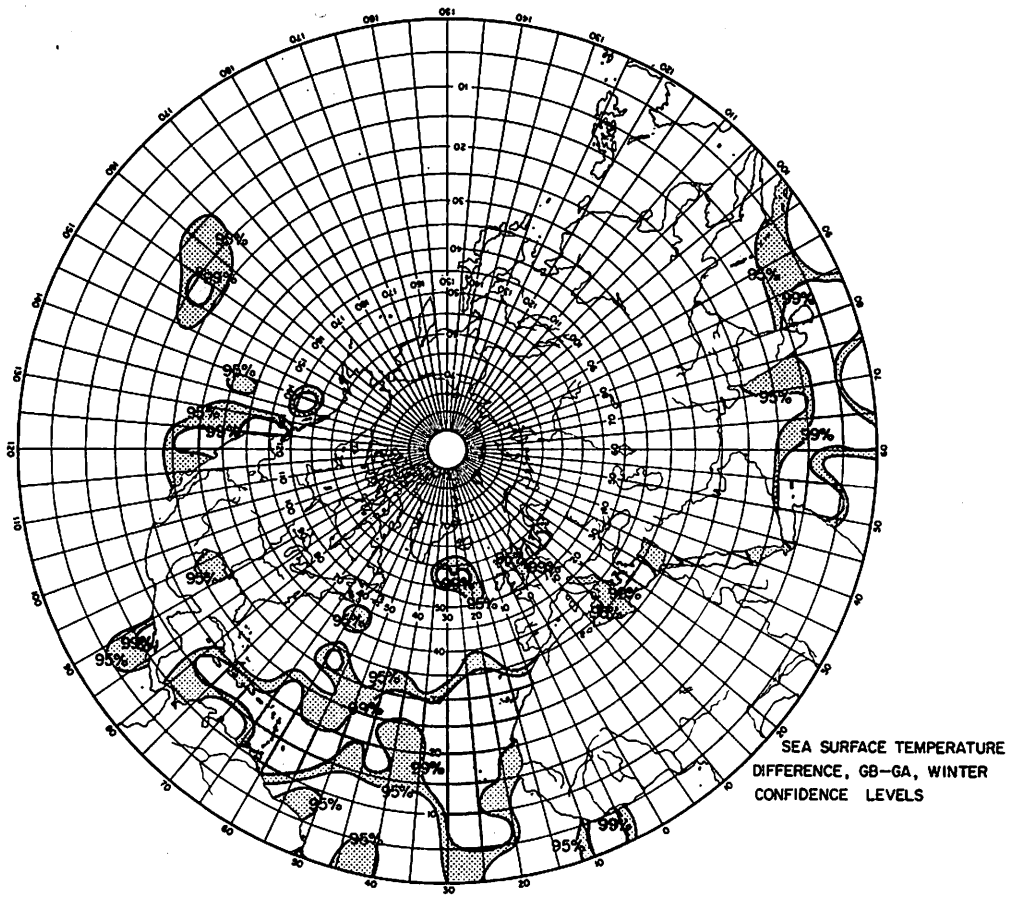

Figure 13. Two tailed t test of SST differences in Fig. 12. Shaded areas are above the 95% confidence level.

eastern tropical Pacific near 120°W from the equator to 10°N. A large area of positive differences covers most of the North Pacific. It should be noted, however, that data coverage from the Pacific has only been fairly adequate since World War II. (See Appendix D for SST observational density). From Figure 13 it can be seen that the differences off the coasts of Baja, California and Central America as well as the ones in the Hawaiian region are significant above the 95% level. Another area of large significant negative differences also exists in the Indian Ocean.

From the data presented in Figures 12 and 13, it is clear that the oceans of the world are closely related in some way to the atmospheric processes previously described. The first and most obvious way SST's respond to atmospheric forcing is through latent and sensible heat loss which is directly proportional to the wind speed as described by the bulk aerodynamic equations listed in Appendix A. Therefore, with an increase in wind, an increase in latent and sensible heat loss at the ocean's surface can be expected and lower SST's result (Bunker, 1976). A second control over SST's which is also wind-related is upwelling. This process occurs when wind stress is applied to an ocean surface. Ekman drift of the surface water then begins, and vertical motion of subsurface water is necessary to replace the water removed at the surface (Hastenrath, 1977; Bjerknes, 1960). Since subsurface water temperatures are generally less than surface temperatures, lower SST's are observed in areas of increased wind stress (Brown, 1963).

A third factor influencing SST's is radiational exchange at the ocean surface (see Appendix A for radiation exchange equation).

One of the major controls on the radiation balance is cloudiness -- more clouds result in less solar radiation reaching the ocean, and an observed decrease in SST even though cloud cover does tend to hold in some of the outgoing longwave radiation (Bunker and Worthington, 1976). Finally, local SST's can change depending on advection rates or positions of ocean currents (Stommel, 1970). Looking again at Figure 12, it is probable that the large negative SST differences seen across the tropical Atlantic are due to the stronger trade winds described in Section 4 which increase losses of latent and sensible heat and enhance vertical mixing.

The small area of positive differences between 5^{o} and 10^{o}N, even though it is not statistically significant, is of interest because it coincides almost exactly with an area of net oceanic heat loss given by Bunker and Worthington (1976) (see Fig. 14.1) and Hastenrath and Lamb (1978) (Fig. 14.2-14.4). Bunker (1976) explains that this is an area very sensitive to changes in cloud cover from the ITCZ which lies near this region during winter as seen in Figures 14.5-14.7 (Hastenrath and Lamb, 1977). If the cloudiness maximum associated with the ITCZ was further south during GB winters, this area would receive more solar radiation and be relatively warmer than during GA winters, thus producing the positive SST difference seen in Figure 12. Results presented in the preceding section indicate that the ITCZ shifts further south over the African continent during GB winters. Recent evidence presented by Lamb (1978) suggests that shifts in position of the ITCZ over Africa are probably linked to similar shifts over the tropical Atlantic. It does seem a possibility in this case, then, that an ITCZ shift to the south over

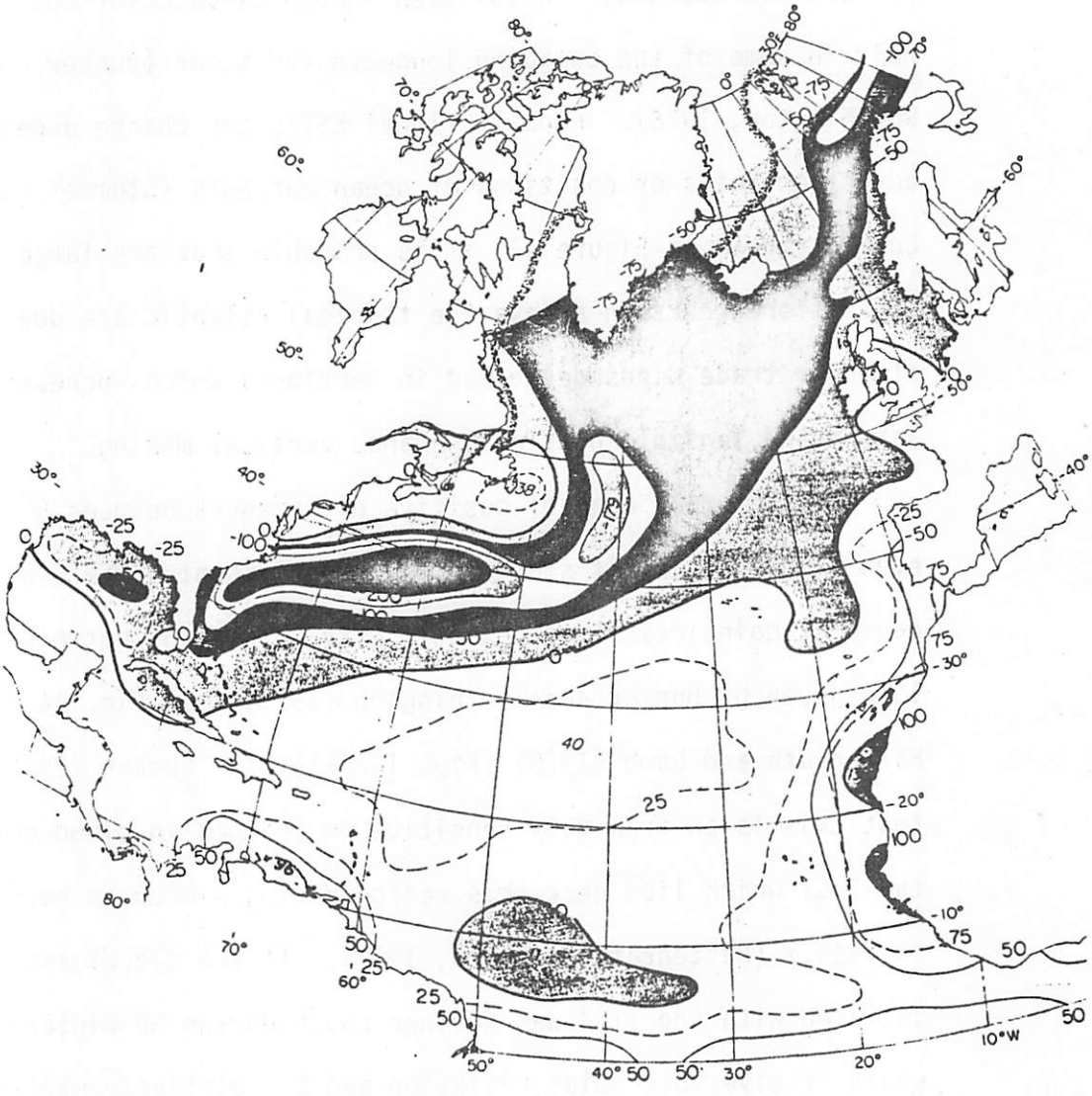

Figure 14.1 Annual average heat gain $\left(W\ m^{-2}\right)$ for the North Atlantic. Shaded areas indicate negative heat gain (after Bunker and Worthington, 1976).

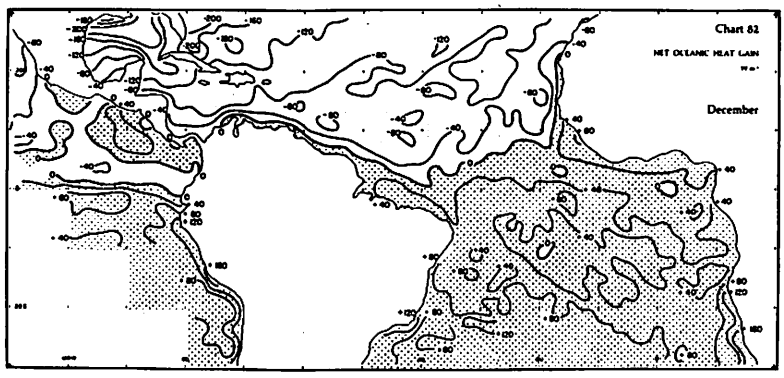

Figure 14.2 Net oceanic heat gain $\left(W\ m^{-2}\right)$ for the tropical Atlantic, December (after Hastenrath and Lamb, 1978).

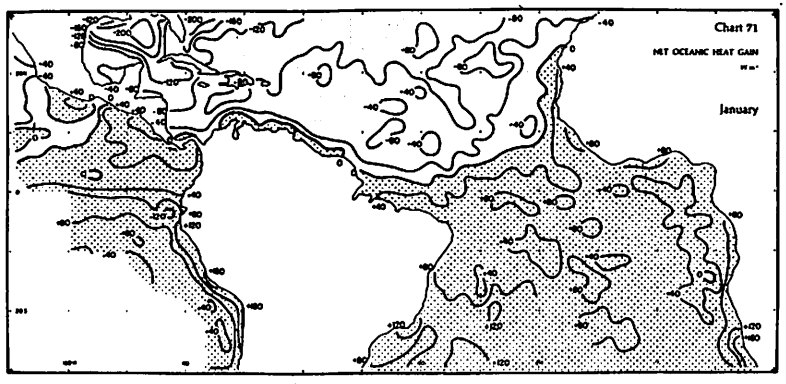

Figure 14.3 Same as Fig. 14.2, except for January.

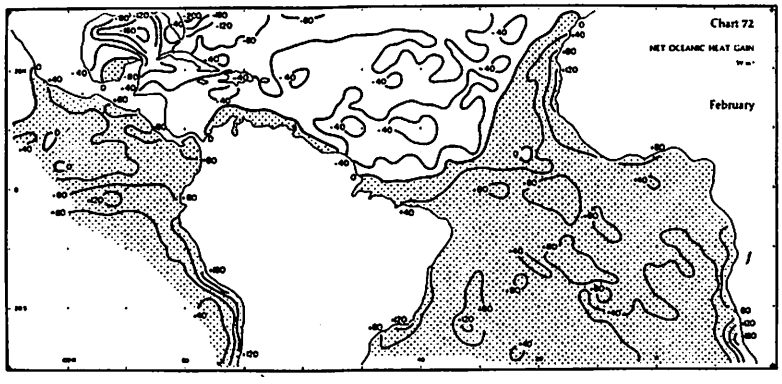

Figure 14.4 Same as Fig. 14.2, except for February.

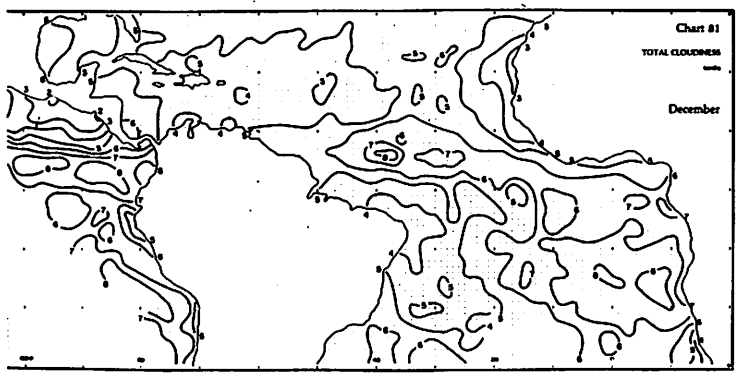

Figure 14.5 Total cloudiness in tenths for the tropical Atlantic, December (after Hastenrath and Lamb, 1977).

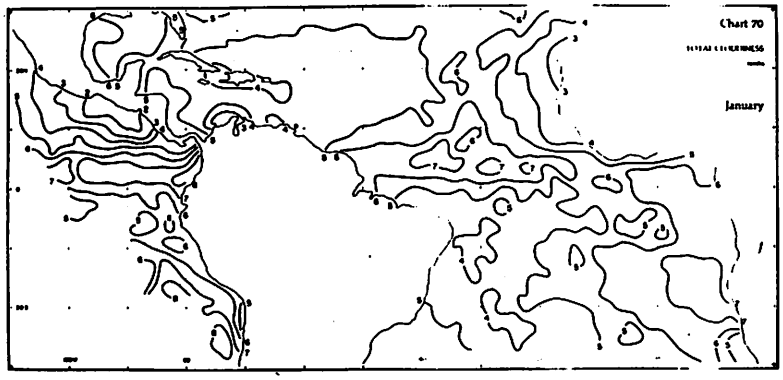

Figure 14.6 Same as Fig. 14.5, except for January.

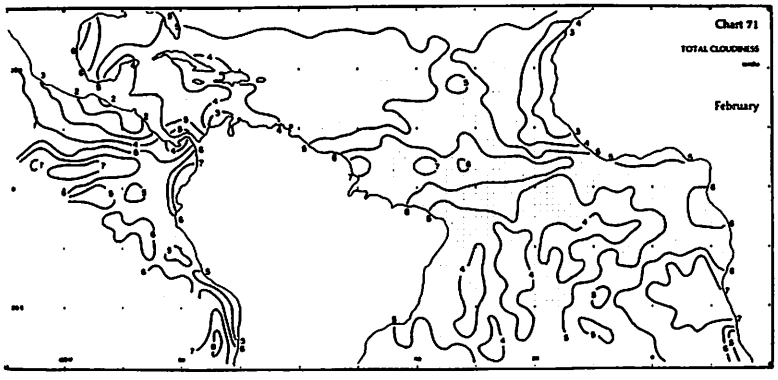

Figure 14.7 Same as Fig. 14.5, except for February.

Africa during GB winters could be accompanied by a similar shift over the tropical Atlantic, and vice versa for GA winters.

Another small area of positive differences occurs just off the Georgia coast. This area on first inspection seems unreliable because of the unusually large SST difference (almost a 1.5^{o}C gradient between it and neighboring values) plus the fact that there are less reported data there than for the surrounding regions. However, two points can be made to suggest that the SST in this area is not spurious. First, it must be remembered that the SST data used here are smoothed area averages for each 5^{o} square of latitude and longitude. Observations taken for the area in question can only be included from a small oceanic corner of the 5^{o} square bounded by 80^{o} to 85^{o}W longitude, and 30^{o} to 35^{o}N latitude. This fact automatically increases the resolution of the data coverage since only a small segment of that particular 5^{o} square lies over the ocean. Secondly, Figure 15 shows that the small portion of this 5^{o} square contains an extremely steep gradient of the contours of surface temperature resulting from the rapid decrease of SST between the core of the Gulf Stream and the U.S. coast. There is no other 5^{o} square with similar resolution containing such a steep gradient because, as can be seen in Figure 15, the strongest gradient lies very near the coast and other 5^{o} squares in the region have sufficiently large areas to include expanses of warm water to the east of the tightest gradients. Due to the smoothing and averaging, the larger areas of warmer water in the other 5^{o} squares would effectively drown out any signal from changes in gradient between the Gulf Stream core and the coast. The exceptions would be 5^{o} squares lying further north where the Gulf

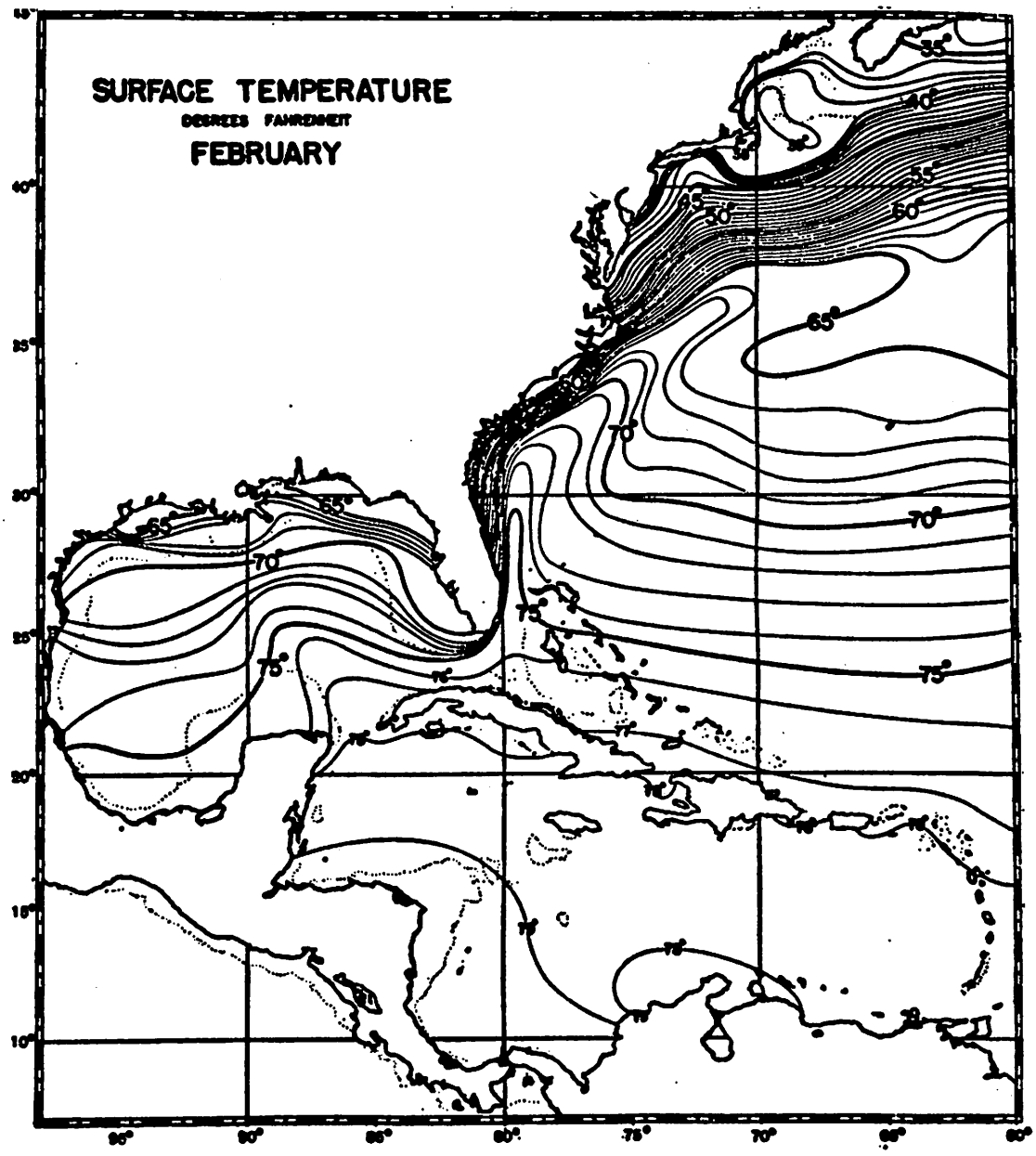

Figure 15. Sea surface temperature in the western North Atlantic for February (after Fuglister, 1947).

Stream gradients occupy a significant portion of their areas. This is exactly where a band of positive differences lies to the north of Cape Hatteras extending two thirds of the way across the North Atlantic, areas of which are statistically significant at the 95% level. This would seem to hint at the possibility that the entire tropical and subtropical Atlantic gyre (refer to Fig. 16) is expanded radially outward during GB winters. If this were the case, the SST gradient between the core of the Gulf Stream and the United States east coast would be pushed west giving a positive SST difference in the area off the Georgia coast. Similarly the increased radial extent of the gyre would shift the SST gradient further north near 40°N giving the positive SST differences seen in Figure 12 in that region.

A possible explanation for radial expansion of the gyre in GB winters could be traced to the stronger trade winds observed in the Atlantic in those winters. As stronger trades remove heat from the central Atlantic, upwelling takes place, isotherms move upward, and the surface current layer would be compressed. To conserve mass, the North Atlantic gyre would expand radially outward and, to conserve vorticity, slow down as evidenced by the slower Gulf Stream speeds observed in GB winters. However, there is no evidence to support the contention that the surface current layer compresses in the manner necessary to maintain an outward radial expansion of this magnitude.

The band of positive differences across the North Atlantic near 40°N, and the decreased Gulf Stream flow during GB winters, could also be explained in terms of wind stress. In Figure 4 the area from 20-40°N is covered by negative correlations indicating

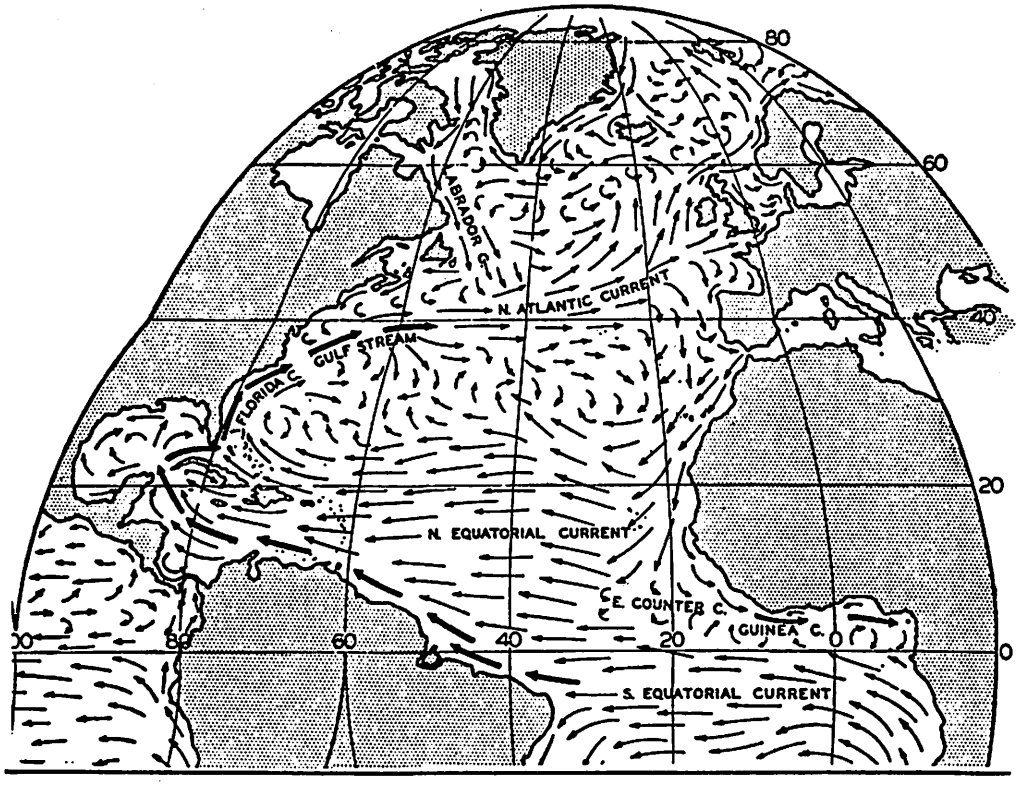

Figure 16. Surface currents of the North Atlantic Ocean (after Sverdrup et al., 1946).

that, since this is an area of mean westerlies, there are weakened westerlies during GB winters. The sea level differences across the Gulf Stream (Fig. 9) show that the negative differences become larger, and associated Gulf Stream flow slower, as one progresses north up the east coast of the United States. This could be due to change in the angle of the section with reference to the coast and current, but could also be due to weakened westerlies northeast of Cape Hatteras which would slacken Gulf Stream outflow. Decreased wind stress in that area would also result in a decrease of latent and sensible heat loss and vertical mixing which could produce the higher SST's seen there during GB winters.

The pattern of SST's in the Bermuda-east coast United States region suggests that the sea level variations observed in the preceding section may be due to steric effects. To investigate this possibility, sea level changes were computed for the Bermuda and east coast United States stations using observed SST's for GB and GA winters. The mixed layer is assumed to be isothermal and the water temperature at the surface representative of the temperature throughout the mixed layer. Based on observations, the mixed layer in winter near Bermuda is assumed to be 300 meters, and for the east coast it is taken to be 200 meters (Stommel, 1960). It should be noted that mixed layer processes change as the total water depth decreases near the coast, but a 200 meter mixed layer is used here to obtain a relative measure of sea level change. Salinity near Bermuda is taken to be 36 $^{0}/_{00}$, and 35 $^{0}/_{00}$ near the coast (Stommel, 1960). For the Bermuda vicinity, the SST observed during GB winters is 19.6^{o}C and 20.1^{o}C for GB winters. Using a chart of temperature versus salinity

(Bryan and Cox, 1972), a density of 1.0257 g/cm^3 was obtained for the GB winters, and 1.0255 g/cm^3 for GA winters. Assuming a one centimeter square column of water in a 300 meter mixed layer has a constant mass of 3 x 10^4 g, the height of the column is given by

$$H = \frac{(3 \times 10^4 \text{ g})(1 \text{ cm}^2)}{\rho} \qquad (1)$$

where H is the height of the column in centimeters and ρ is the density of that column. Computing H for GB and GA and then differencing the two quantities (GB minus GA) give ΔH = 5.7 cm at Bermuda. The negative sign means that sea level is higher there during GA winters.

Following the same procedure for the ocean areas off the east coast of the United States west of Bermuda and using a GB SST of 18.9^{o}C and a GA SST of 17.6^{o}C, the respective densities for the same salinities are 1.0251 g/cm^3 and 1.0255 g/cm^3. Substituting these densities into Equation 1 and differencing GB minus GA, the change in height is found to be ΔH = + 7.6 cm. The positive sign indicates lower sea levels during GA winters. Therefore, the net change of sea level for GB minus GA between the east coast of the United States and Bermuda, computed purely from steric considerations, is -13.31 cm which is very close to the largest observed differences seen in Figure 9. Therefore, Lisitzin and Pattullo's (1961) contention that steric effects are the most important determination of sea level variation south of 40-45^{o}N seems to be valid in this case.

In the Pacific, the large band of negative and, in some areas, statistically significant SST differences (see Fig. 13) stretching

from Baja, California westward past Hawaii toward the Philippines can again probably be attributed to the increase of northeast trade wind intensity during GB winters causing cooling through more latent and sensible heat flux and increased vertical mixing. Moving south toward the equator, data become more and more sparse, but the area of positive SST differences near $120^{o}W$ and south of $10^{o}N$ is worth noting because, as seen earlier, the theories of Bjerknes and others ascribe vital importance to SST's in this area of the Pacific in terms of eventual links to midlatitude weather. Another major feature of the Pacific SST differences in Figure 12 is the huge area of positive differences extending most of the way across the northern Pacific. Due to high variance and data scarcity, these large differences are not statistically significant, but again are of interest in light of other investigators' theories of Pacific Ocean interactions between the tropics and midlatitudes. It is interesting to note that the pattern of large positive SST anomalies in the North Pacific during GB winters and negative ones for GA winters has been verified by several case studies of individual winters such as the GA winter of 1957-58 (Bjerknes, 1966), the GB winter of 1971-72 (Namias, 1972), and the GA winter of 1976-77 (Namias, 1978).

Chapter 8

UPPER AIR PHENOMENA

The position of the subtropical jet stream is thought to mark the poleward edge of the Hadley circulation and is an important indicator of the amount of westerly momentum being transferred from the tropics to the midlatitudes (Palmén and Newton, 1969; Krishnamurti, 1961b). In this section the position of the subtropical jet stream at 300 mb, as defined by the west wind maximum at that level, is compared between GB and GA winters.

The subtropical jet stream is a relatively constant feature whose axis ranges in latitude from 20^{o}N to 35^{o}N and whose maximum speeds occur near 300-200 mb (Krishnamurti, 1961a). Weinert (1968) found that the average subtropical jet axis in the Australian region varies by no more than 6^{o} from month to month. Murray (1960) explains large local variations of monthly mean flow in the subtropical jet by displacements of a few degrees in latitude without regard to changes in velocity. However, Troup (1961) adds that changes in intensity can also play a role in addition to small shifts in position of the jet axis.

Data from the NCAR upper air tapes were used here but 300 and 200 mb data only go back as far as 1962. Since 1962, there have been only six seesaw winters. Therefore, 700 mb temperature data dating back to 1947 (9 seesaw winters) were used instead to provide more cases and to give an indication of the position of the subtropical jet stream at upper levels by invoking the thermal wind relationship

(see Appendix A for thermal wind equation) where temperature gradients at lower levels in the atmosphere are indicative of geostrophic flow at upper levels. To verify that this approach was valid, 5^{o} latitudinal 700 mb temperature gradients were correlated to 300 and 200 mb geostrophic u component winds at 5^{o} grid points. Both levels had high correlation values, but the 300 mb ones were slightly higher (Fig. 17). Correlation coefficients are well above .7 (and in some areas above .9) virtually all around the lower latitudes of the Northern Hemisphere, except in a small area north of Palestine where unreliable upper air data could be a factor. The Himalayan area was not analyzed since this region rises above 700 mb. It should be safe to assume, therefore, that 700 mb latitudinal temperature gradients can give an indication of u component 300 mb geostrophic winds.

The difference map of GB minus GA winter 700 mb temperature gradients and the associated significance levels are shown in Figures 18a and b. Once again the sign of the difference is indicative of the sign of a GB winter. There is a general tendency toward negative differences between $20\text{-}30^{o}$N with positive differences directly to the north from $30\text{-}50^{o}$N. The most obvious exception to this pattern is over North Africa and Europe where the regions of positive and negative differences are in the opposite sense.

van Loon and Williams (1977) found that a weakening of 700 mb temperature gradients is associated with a southward displacement of the region of most frequent storm tracks. Here, the intensified 700 mb temperature gradient across the North Atlantic during GB winters would indicate that more low pressure centers track further north,

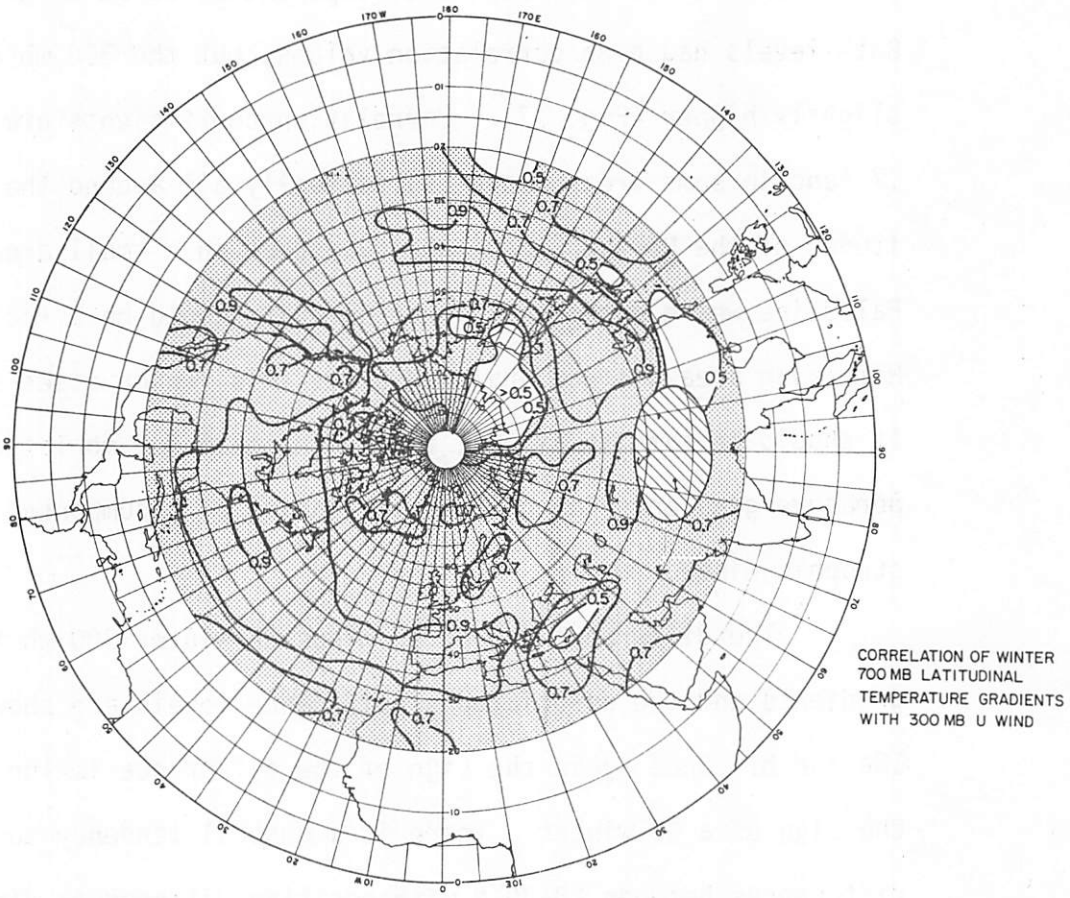

Figure 17. Correlation of winter 700 mb latitudinal temperature gradients with 300 mb U-component geostrophic wind. Stippled areas are above the 95% confidence level.

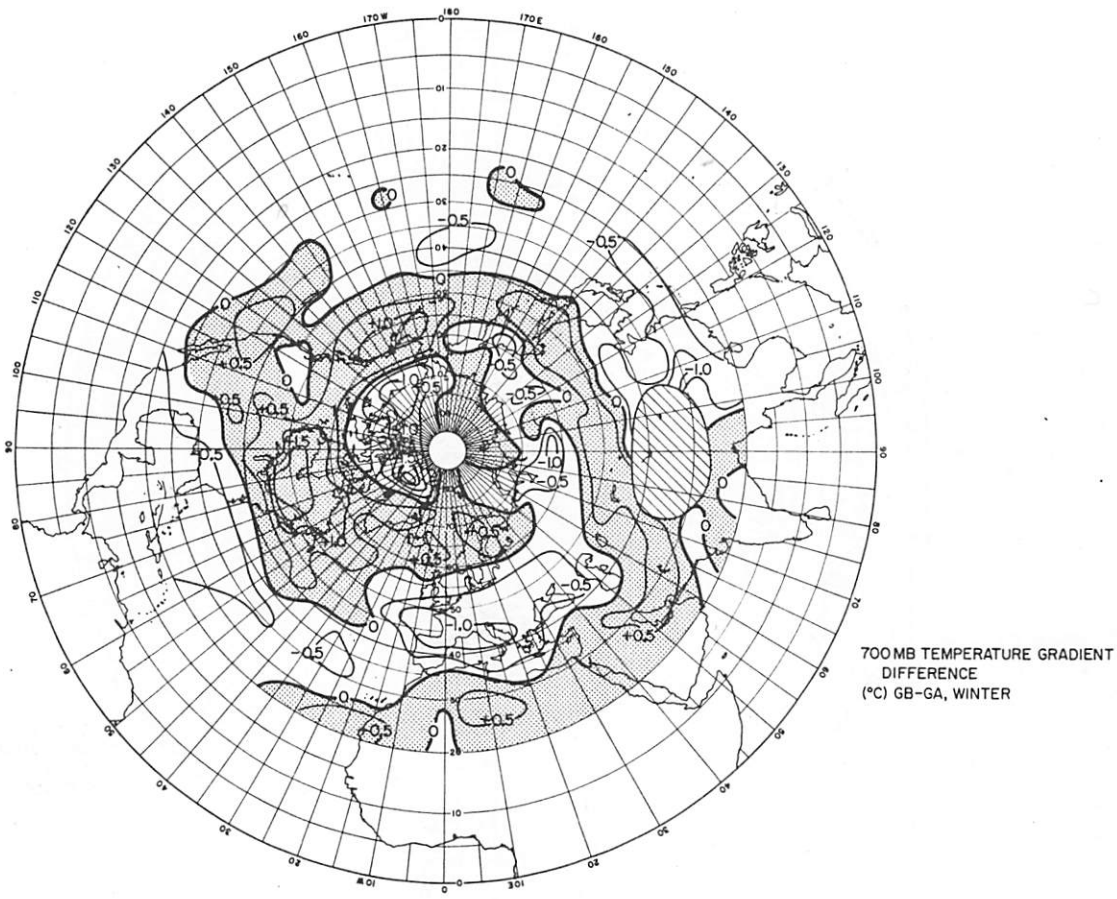

Figure 18.a 700 mb 5^{o} latitudinal temperature gradient difference in ^{o}C, GB minus GA, for nine seesaw winters. Positive differences are stippled.

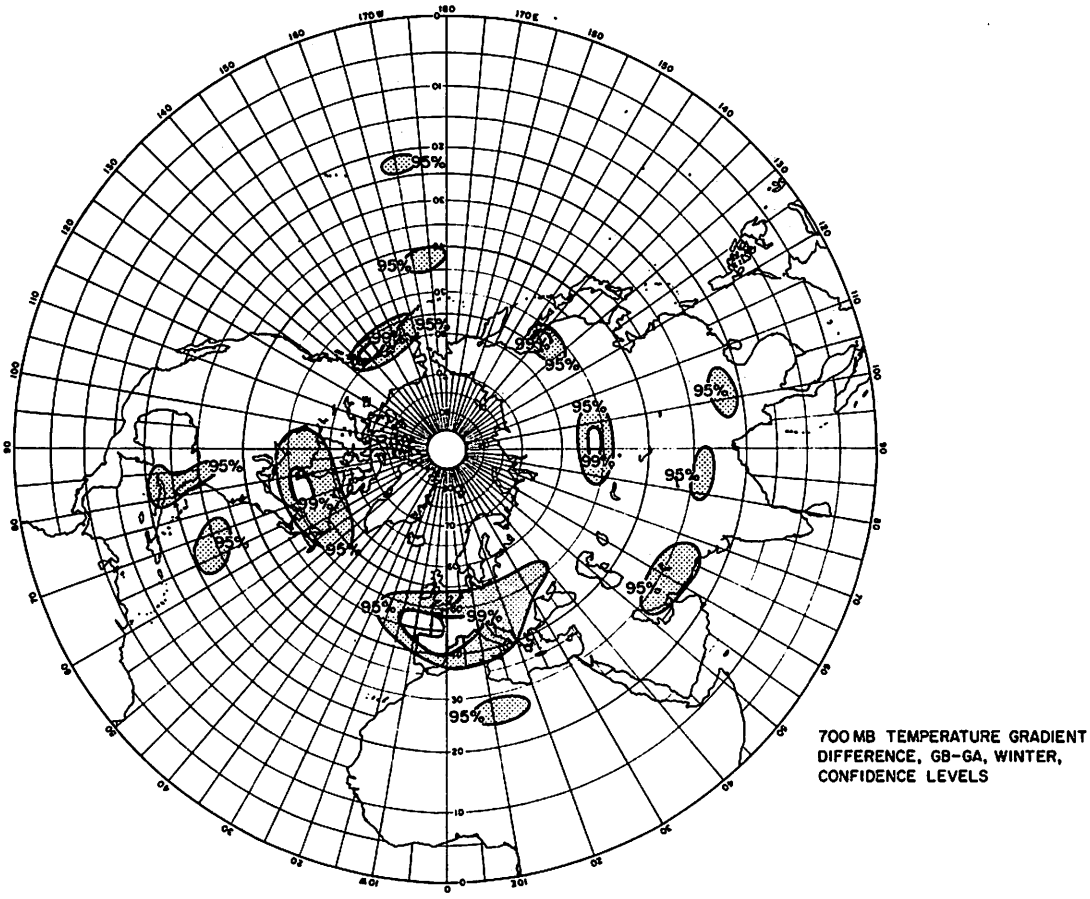

Figure 18.b Two tailed t test for 700 mb temperature gradient differences in part a. Shaded areas are above the 95% confidence level.

which was noted by Rogers and van Loon (1978), resulting in the intensified Icelandic low and the milder winters observed in Europe during the GB mode. In addition, it was noted in Figure 12 that a band of positive SST differences stretch across the Atlantic near $40^{o}N$. This would intensify the SST gradients to the north of $40^{o}N$, weaken them to the south, and coincide with the northward displacement of the 700 mb baroclinic zone and associated storm track path.

Using the 700 mb temperature gradients as indicators of 300 mb u winds leads one to conclude that the 300 mb u wind maximum shifts north in all regions of the Northern Hemisphere, with the exception of a southward shift over Africa during GB winters, and vice versa in GA winters.

Chapter 9

LEADS AND LAGS: SUMMERS AND AUTUMNS PRECEDING AND SPRINGS FOLLOWING SEESAW WINTERS

Sea-level pressure

Sea-level pressure difference maps for the two seasons preceding and the one following seesaw winters were computed as a first step in determining if there are any indications of a following seesaw winter or whether any features persist beyond a seesaw winter. Regions over North Africa, India, and central Asia were not analyzed due to inhomogeneities in the data (Madden, 1976). The SLP difference map, GB minus GA, for summers prior to seesaw winters is shown in Figure 19a. Small positive pressure anomalies are evident in the vicinity of the subtropical highs in the Atlantic and Pacific, as well as over northern Canada. The statistical significance of these differences can be seen in Figure 19b.

Figure 20a is the SLP difference map for GB minus GA lead autumns prior to seesaw winters. As in the preceding map, small positive pressure anomalies appear in the subtropical regions of the Pacific and Atlantic as well as over the Aleutians and northern Canada, with an area of small negative differences over Greenland. Statistical significance associated with these anomalies is illustrated in Figure 20b.

A statistically significant area of positive SLP differences across the North Atlantic can be seen in Figure 21 for springs following seesaw winters. Small positive differences still dominate the subtropical eastern Pacific and subtropical Atlantic.

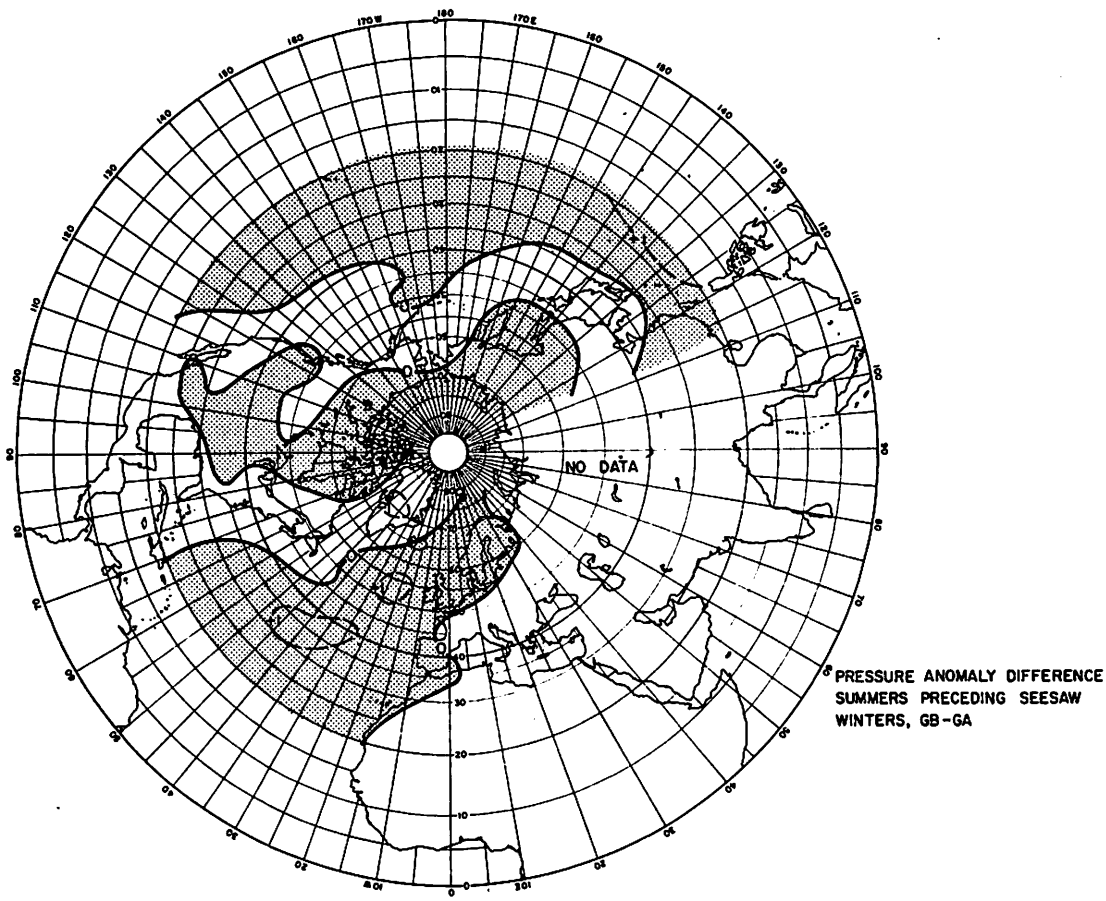

Figure 19.a Sea level pressure difference for summers preceding seesaw winters, GB minus GA. Stippled areas are positive differences. North Africa, India, and central Asia were not analyzed due to unreliable data.

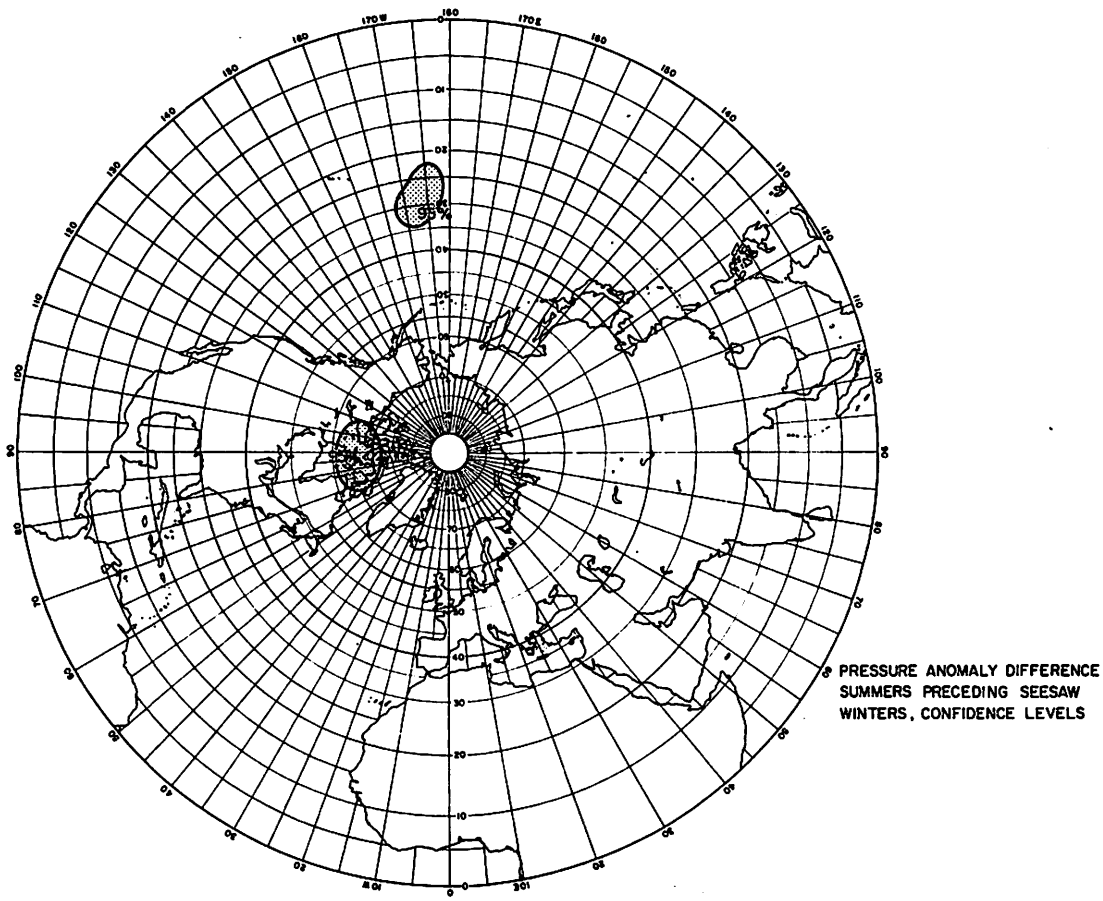

Figure 19.b Confidence levels for the SLP differences in part a. Shaded areas are above the 95% confidence limit.

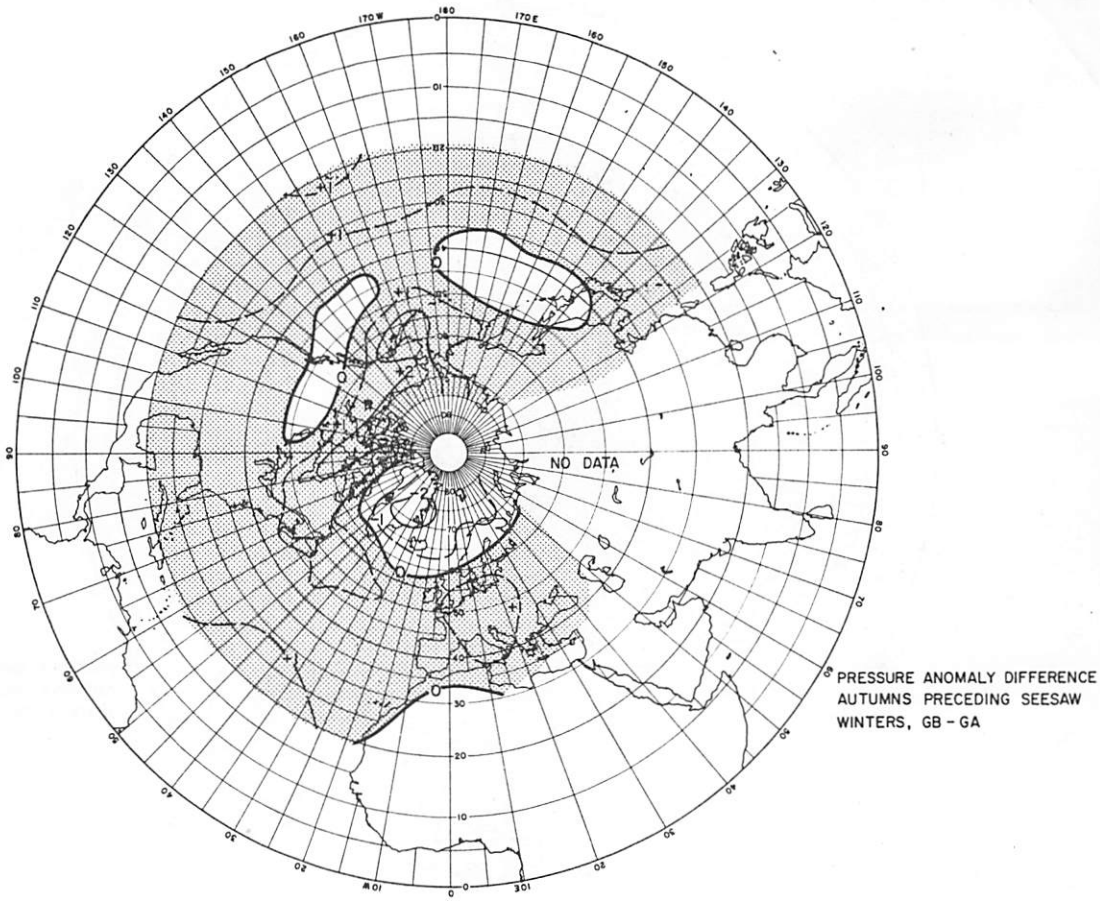

Figure 20.a Same as Fig. 19.a, except for autumns preceding seesaw winters.

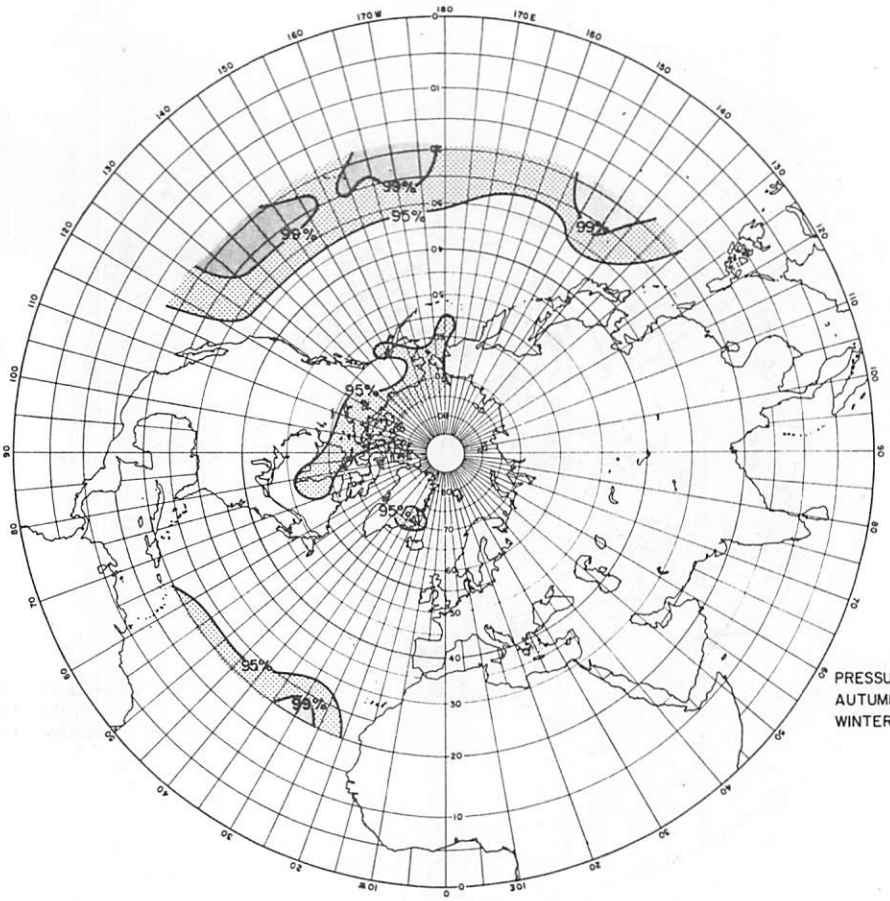

Figure 20.b Same as Fig. 19.b, except for autumns preceding seesaw winters.

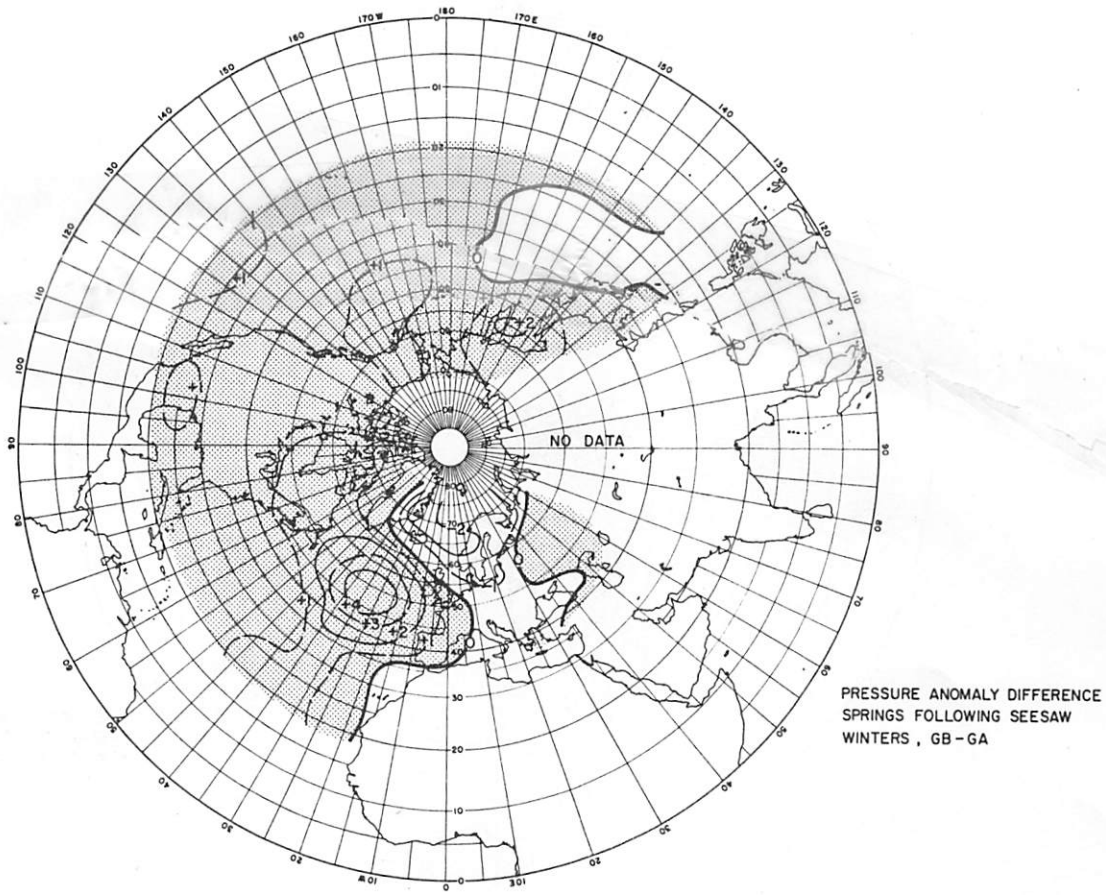

Figure 21.a Same as Fig. 19.a, except for springs following seesaw winters.

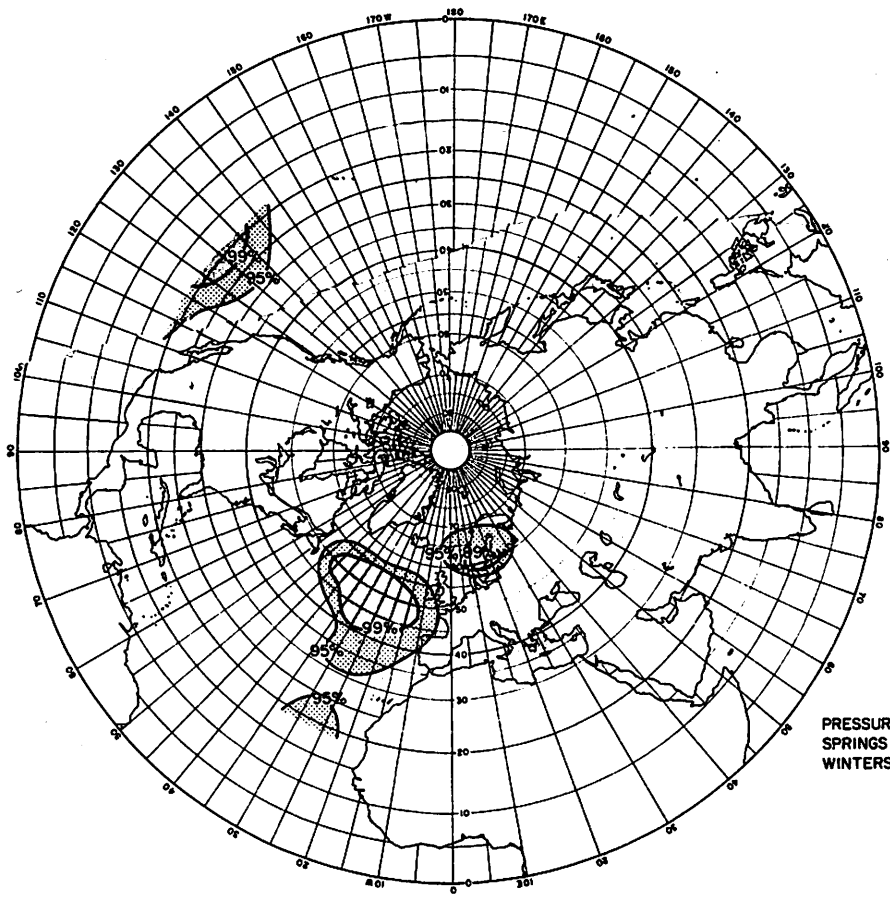

Figure 21.b Same as Fig. 19.b, except for springs following seesaw winters.

Trade winds

In a similar procedure to that carried out in Chapter 5, geostrophic winds were computed from surface pressure differences between pairs of stations or grid points to give an indication of the increase or decrease in trade wind strengths for lead and lag seasons preceding and following seesaw winters. Stations were chosen for the Atlantic and eastern Pacific from the pairs used earlier. In Figure 22, weak increases in trade wind intensity are seen in the Atlantic and Pacific for summers preceding GB winters with the exception of a slight decrease in the northern Caribbean and a large decrease in the South Pacific for the Apia-Rorotonga pair. As was mentioned in Chapter 4, the Apia-Rorotonga and Honolulu-Fanning results should be viewed with a degree of caution due to short record lengths. The percent increases of resultant geostrophic wind for autumns preceding seesaw winters in Figure 23 show fairly large increases for lead GB autumns for the pairs south of 20^{o}N -- Honolulu-Fanning, Honolulu-Cristobal, and Cristobal-Port au Prince. In fact, the magnitude of the increases for those pairs is greater than the values computed for seesaw winters in Figure 5. The same quantity computed for springs following seesaw winters appears in Figure 24. It appears that any discernable responses have weakened for the Pacific pairs as well as for the pairs north of 20^{o}N in the Atlantic where very large increases were seen in GB winters in Figure 5. However, the two Atlantic pairs south of 20^{o}N and the Luanda-St. Helena pair in the South Atlantic still show fairly large percent increases in trade wind strength for springs following GB winters.

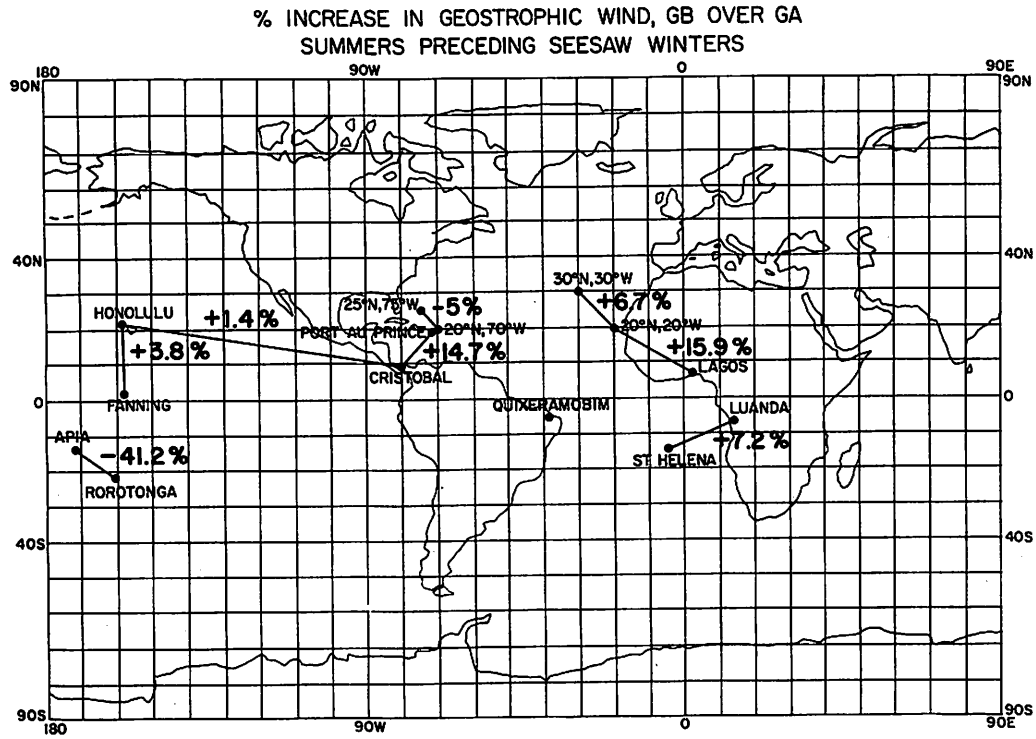

Figure 22. Same as Fig. 5, except for summers preceding seesaw winters.

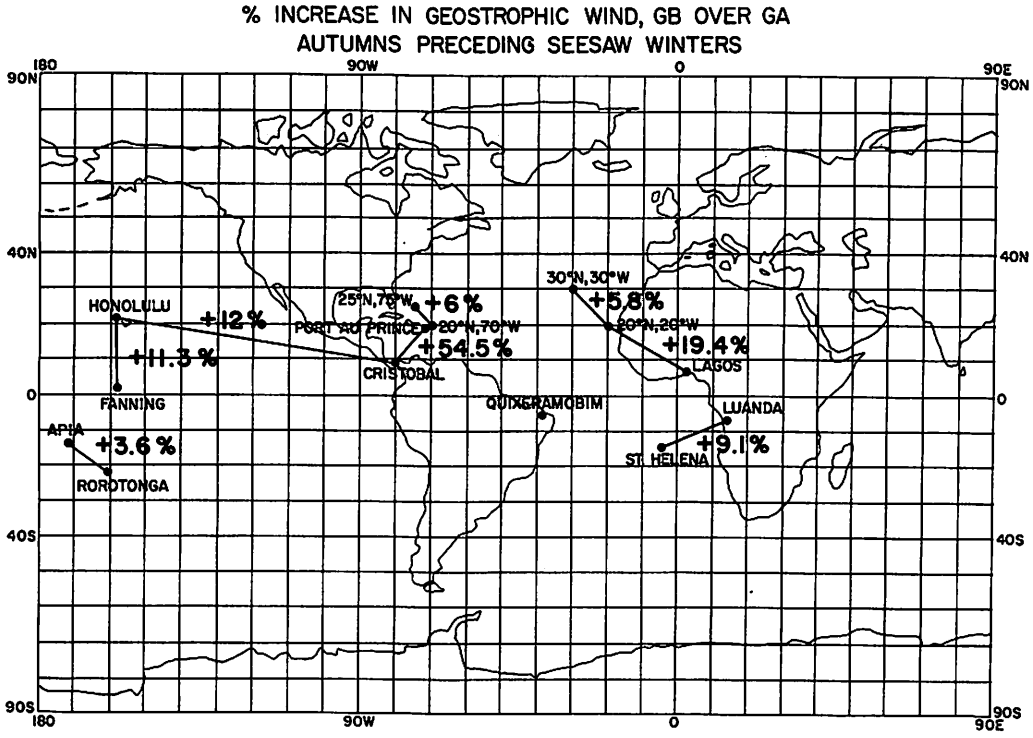

Figure 23. Same as Fig. 5, except for autumns preceding seesaw winters.

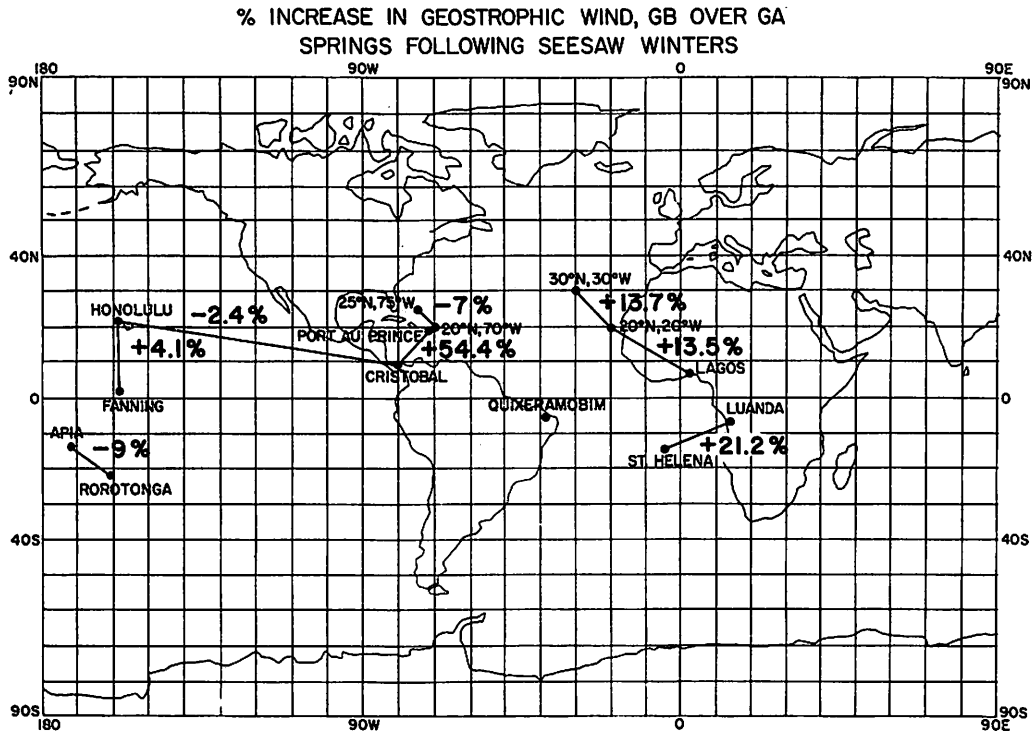

Figure 24. Same as Fig. 5, except for springs following seesaw winters.

Sea levels as indicators of Gulf Stream intensity

Four of the eight pairs used in Chapter 6 were chosen to examine Gulf Stream response in seasons preceding and following seesaw winters. Differences were computed in the same way and appear in Figures 25-27, GB minus GA, for summers and autumns preceding and springs following seesaw winters. It can be seen that all pairs register negative differences in all the lead and lag seasons with the exception of the lag spring Bermuda-Jacksonville pair in Figure 27. Following similar arguments presented in Chapter 6, this would seem to indicate that the Gulf Stream is flowing at a reduced rate in seasons before and after GB winters.

Sea surface temperatures

Sea surface temperature differences were computed in the same manner as in Chapter 6 for lead seesaw summers and autumns and lag seesaw springs and appear respectively in Figures 28a, 29a, and 30a with associated statistical significance levels in part b of each figure. The most persistent feature present on all the difference maps as well as on the winter SST difference map in Figure 13 is the area of negative differences across most of the tropical Pacific, Atlantic, and Indian Oceans indicating cooler SST's during seasons before, during and after GB winters. One interesting region of positive differences that appears on all the SST difference maps is near $120^{o}W$ between the equator and about $8^{o}N$. Another positive difference area lies in the North Pacific. It expands and intensifies from season to season while it slowly moves away from the west coast of the United States. A third group of positive differences spreads across the North Atlantic near $40^{o}N$ as the seasons progress. A final

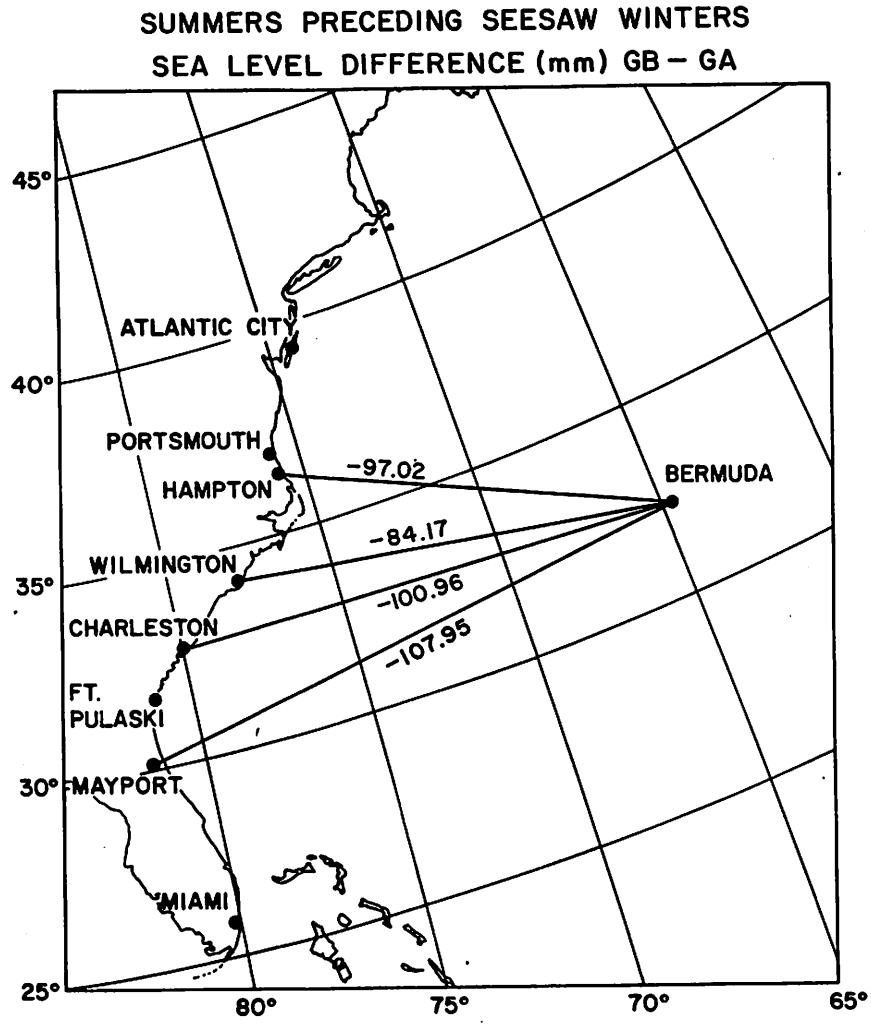

Figure 25. Same as Fig. 9, except for summers preceding seesaw winters.

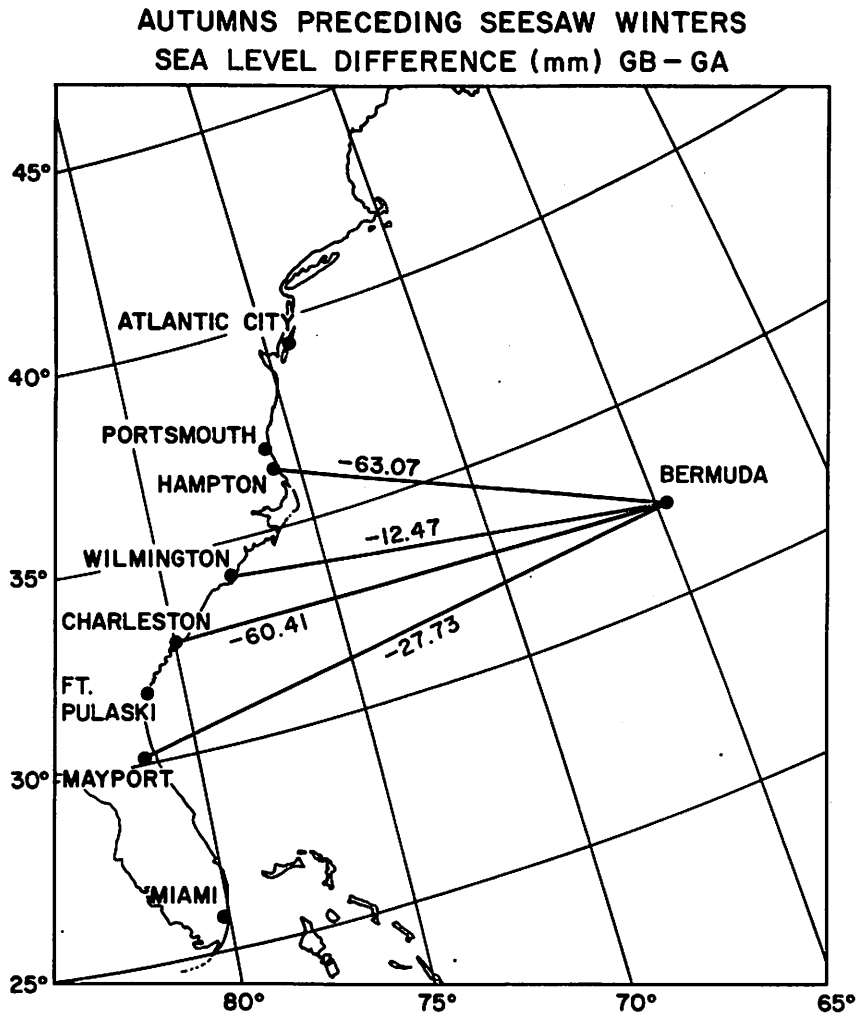

Figure 26. Same as Fig. 9, except for autumns preceding seesaw winters.

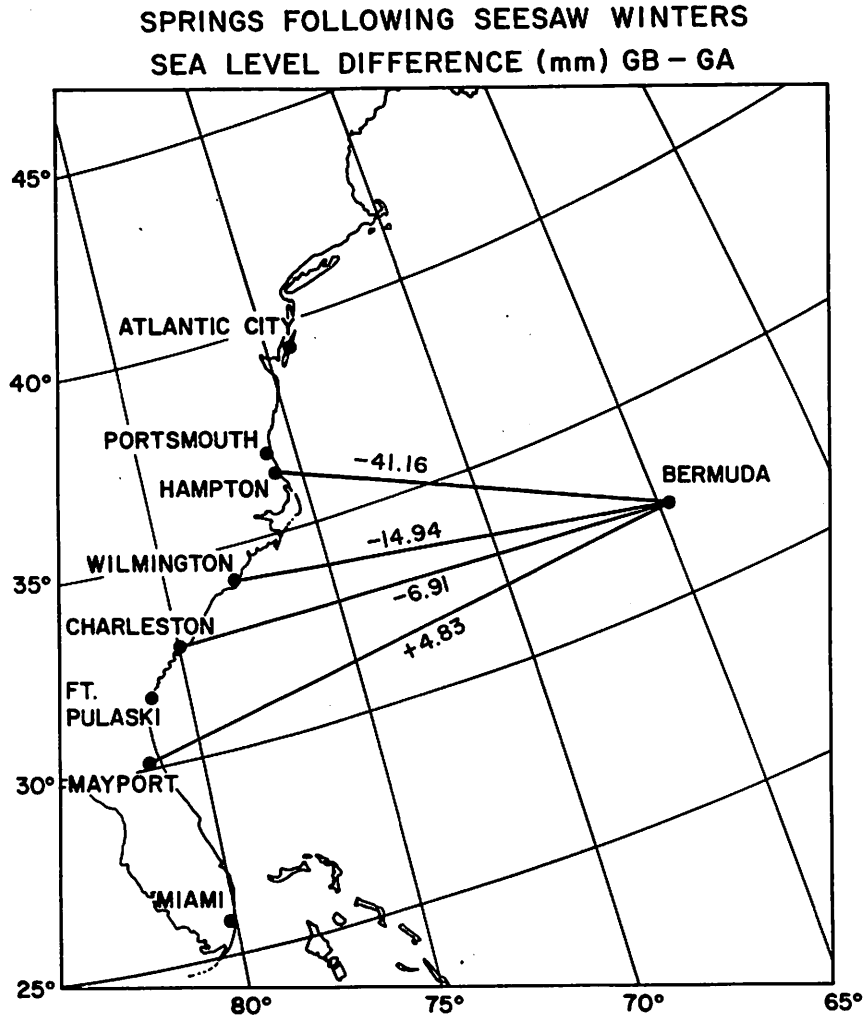

Figure 27. Same as Fig. 9, except for springs following seesaw winters.

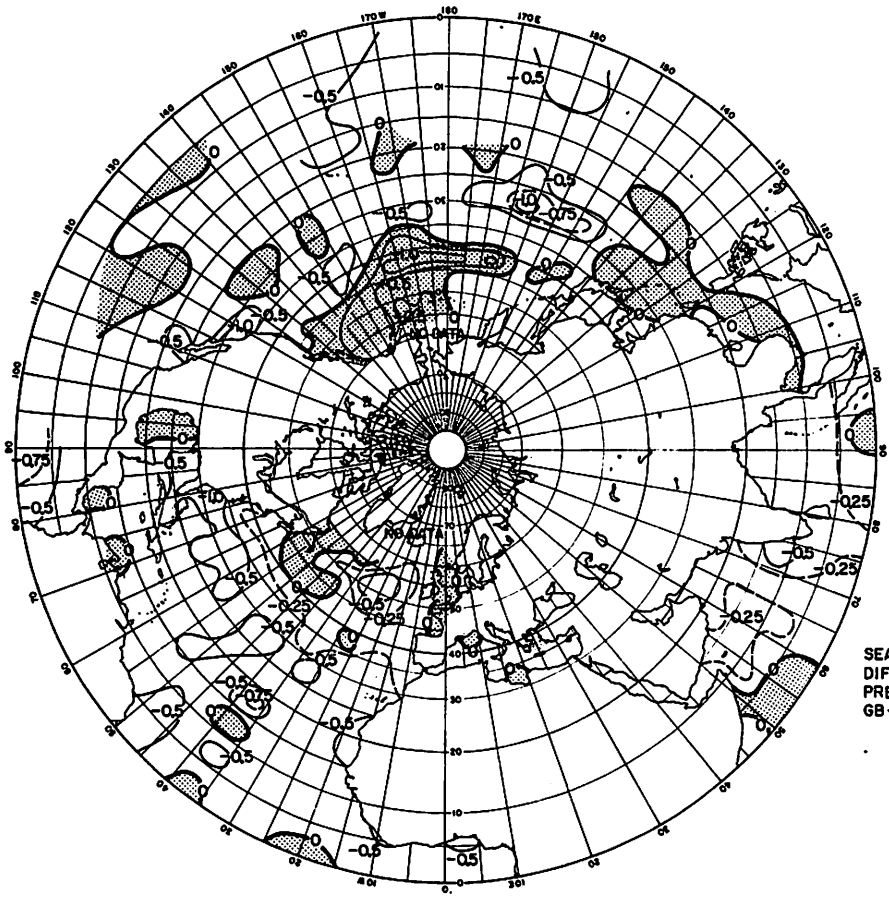

Figure 28.a Same as Fig. 12, except for summers preceding seesaw winters.

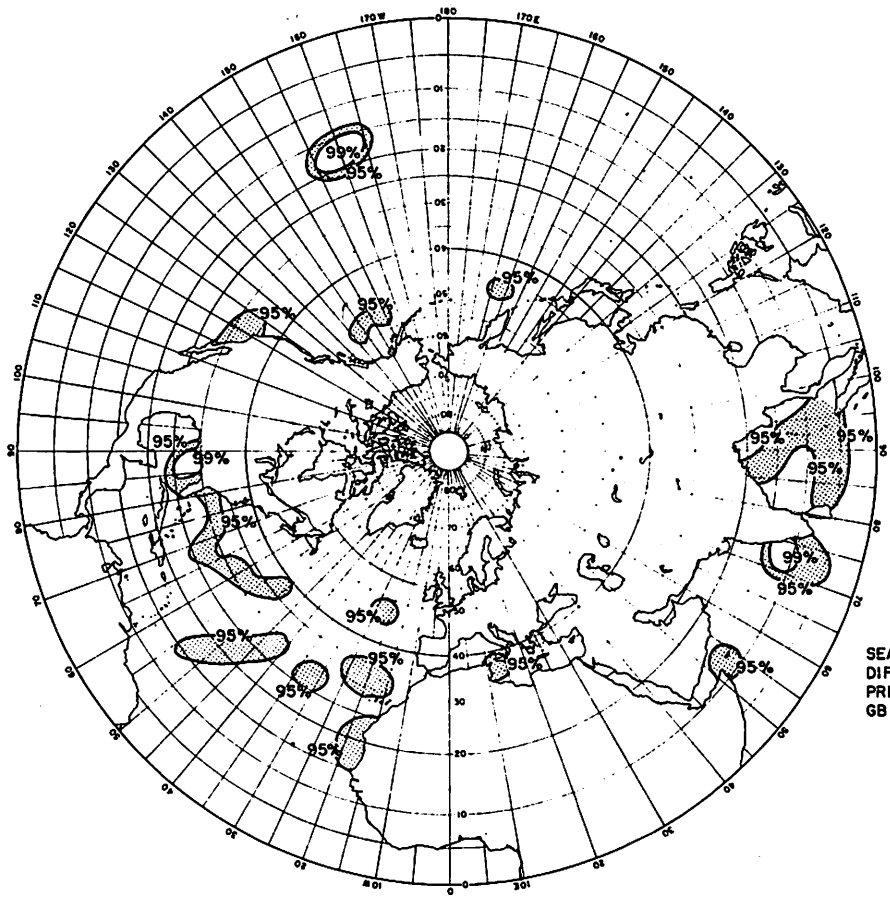

Figure 28.b Same as Fig. 13, except for summers preceding seesaw winters.

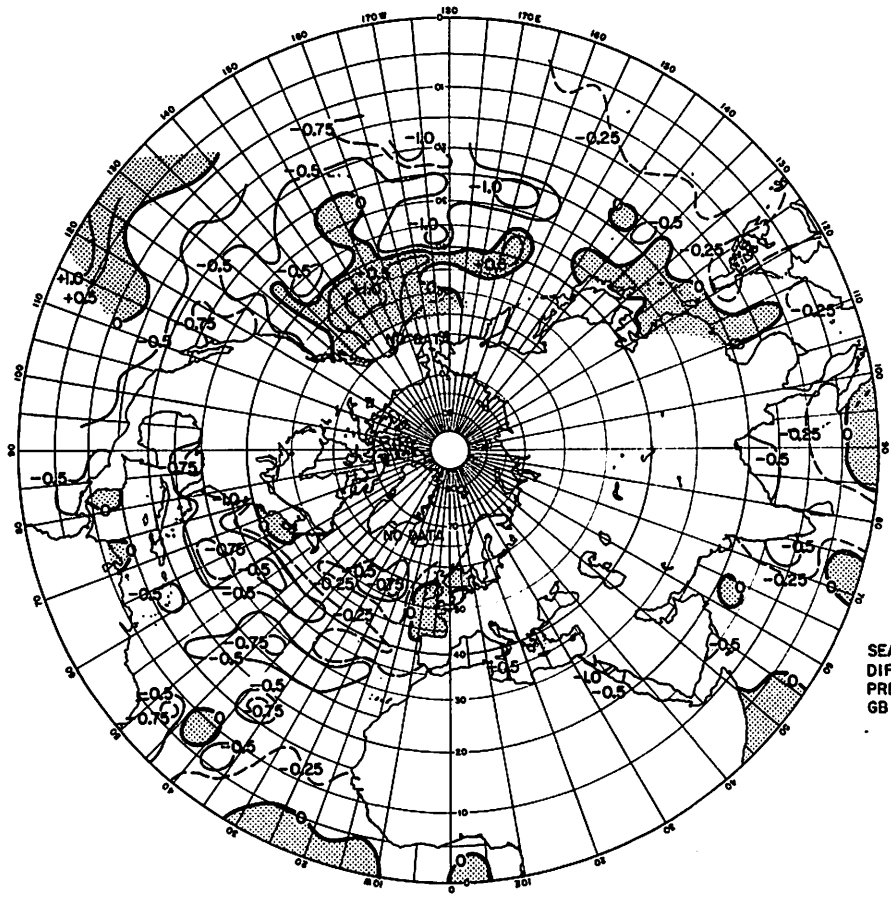

Figure 29.a Same as Fig. 12, except for autumns preceding seesaw winters.

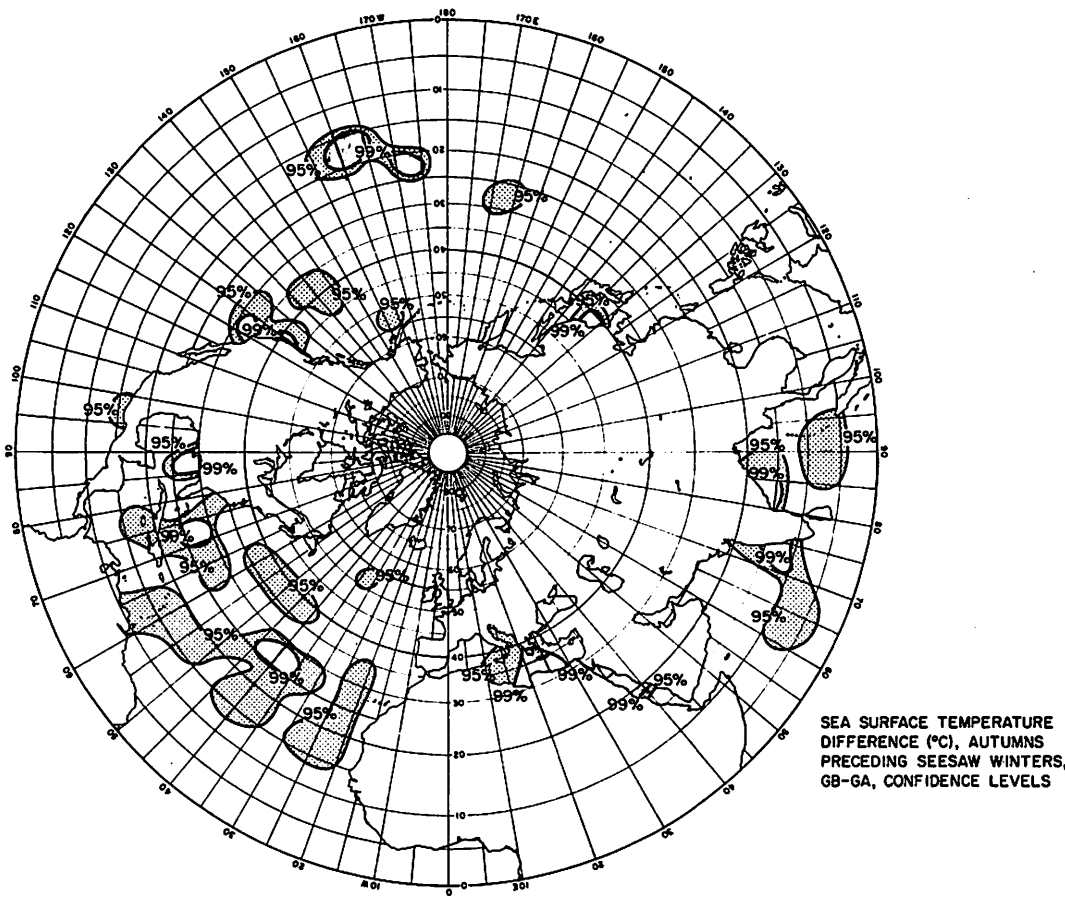

Figure 29.b Same as Fig. 13, except for autumns preceding seesaw winters.

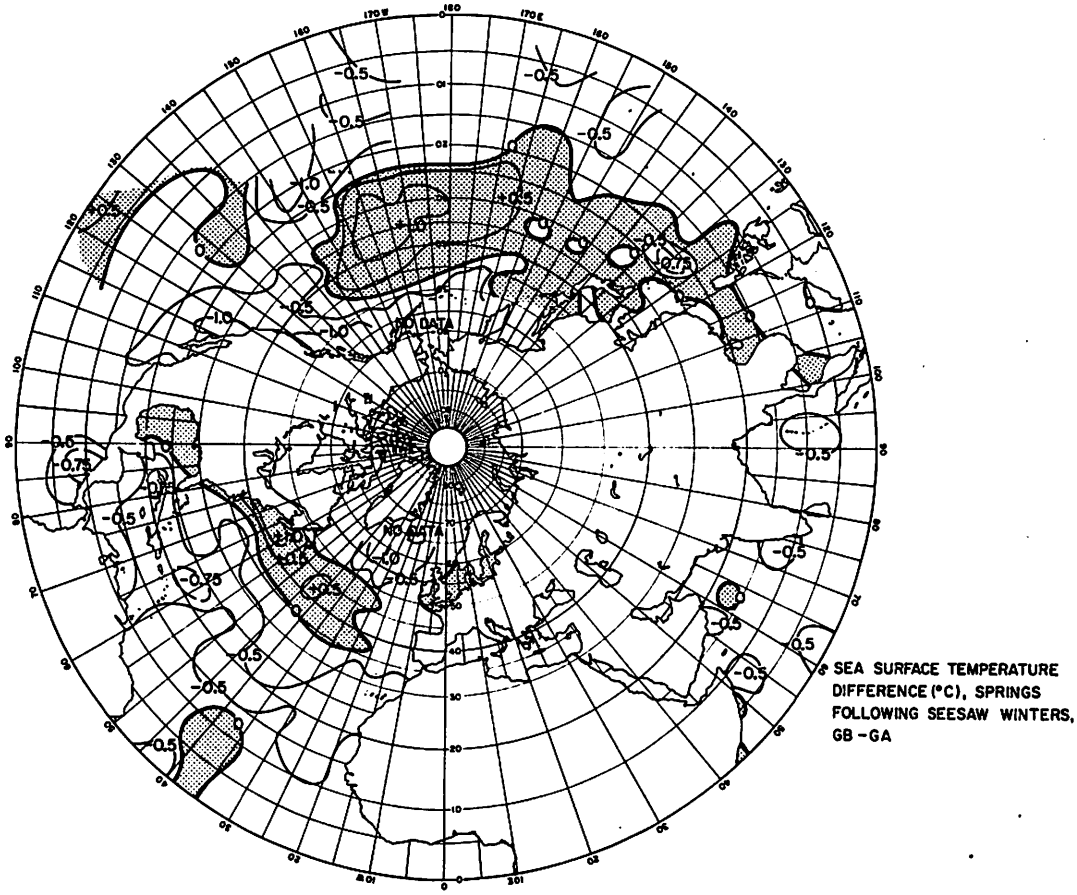

Figure 30.a Same as Fig. 12, except for springs following seesaw winters.

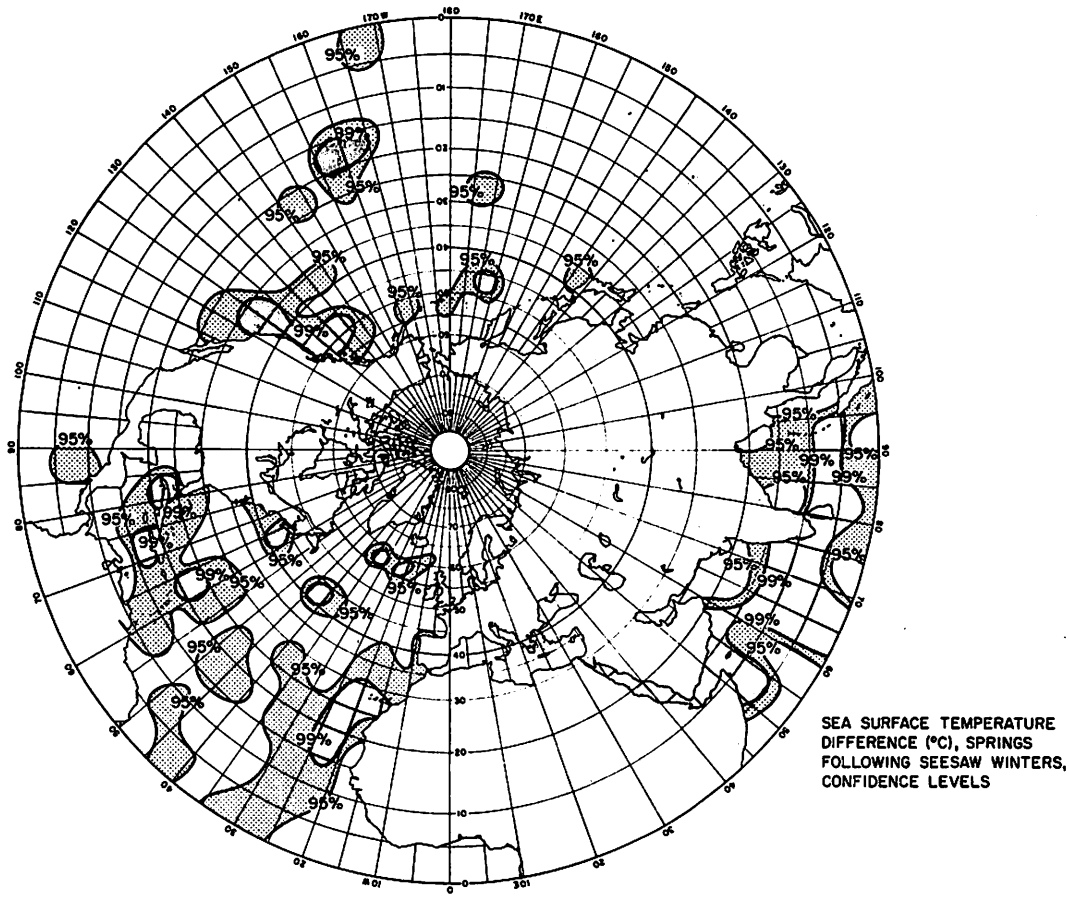

Figure 30.b Same as Fig. 13, except for springs following seesaw winters.

area of interest is near 40°W in the tropical Atlantic. Here, a small area of positive differences persists in the region of ITCZ cloudiness discussed earlier through all the seasons represented in Figures 12, 28, 29, and 30.

Discussion of lead and lag seesaw season results

From the preceding results several points of interest emerge. First, and most obvious, is that the basic ocean-related features appear two seasons before seesaw winters and persist into the following springs. Gulf Stream flow is slower through all seasons and negative SST's dominate the subtropical areas of all three oceans. Mid-latitude SST features also appear two seasons before seesaw winters, then slowly alter form and position as seasons progress (i.e., the positive SST anomalies in the North Pacific and North Atlantic).

The atmosphere does not seem to behave with as much persistence as the ocean even though basic seesaw patterns (of smaller magnitude) are evident in autumns before seesaw winters. Comparing the pressure anomaly differences in Figure 2 (seesaw winters, GB-GA) with the ones in Figure 20 (autumns preceding seesaw winters, GB-GA), positive differences over the Aleutians, extreme northern Canada, and the subtropical areas of the Pacific, Atlantic, and India, as well as negative differences over the Greenland area are common to both, even though the preceding autumn differences are only from one half to one fourth the size of the winter values.

Geostrophic wind flow as indicated by the station pair analysis seems to indicate a building of trade wind intensity in the deep tropics south of 20°N in seasons preceding GB winters except for a possible breakdown in the South Pacific as indicated by the Apia-

Rorotonga pair in preceding autumns with the more northern areas of the trade wind belt reacting strongly only during seesaw winters.

Judging from the SST patterns in seasons preceding the seesaw, it seems possible that some degree of predictability may be possible (e.g., Ratcliffe and Murray, 1970) and preliminary attempts were made to assess the prospects of gaining forecast skill from the SST's in seasons prior to individual seesaw winters. However, it must be remembered that the SST patterns presented here are differences of long term averages. When dealing with the yearly SST's, there are problems inherent with noise and year-to-year variation which tend to make forecasting schemes impractical.

Chapter 10

CONCLUSIONS

It has been established that a number of parameters in the tropics can be linked directly with the major mode of midlatitude circulation called the Greenland seesaw which occurs in approximately 40% of the winters observed over the last 133 years. These observed responses in the tropics include: (1) stronger (weaker) trade winds in the Atlantic and the Pacific during GB (GA) winters; (2) a large highly significant correlation of northeast and southeast trade wind strengths during seesaw winters, but not during other winters; (3) the ITCZ in Africa, as defined by the belt of heaviest precipitation, shifts south (north) during GB (GA) winters; (4) the speed of the Gulf Stream, as implied by sea level differences between Bermuda and U.S. east coast stations, is slower (faster) during GB (GA) winters; (5) significantly lower (higher) SST's are seen across the tropical North Atlantic, North Pacific, and Indian Oceans during GB (GA) winters; (6) the position of the subtropical jet stream (at 300 mb), as defined by 700 mb temperature gradients, shifts north (south) during GB (GA) winters everywhere except over Africa where a shift in the opposite sense occurs; (7) examination of SST's during summers and autumns prior to, and springs following, GB (GA) winters indicates cooler (warmer) tropical Atlantic, Pacific, and Indian Ocean SST's in the lead and lag seasons and a slower (faster) Gulf Stream; (8) seesaw winter SLP anomaly patterns in both the tropics and midlatitudes are weakly present in autumns prior to seesaw winters;

(9) trade winds in the deep tropics (south of 20°N) are stronger (weaker) in the two seasons prior to seesaw winters and especially in autumns preceding seesaw winters; (10) trade winds in the northern fringes of the tropics 20°N-30°N seem to react strongly only during seesaw winters, and weakly in the lead and lag seasons. (See Table 4 for summary of results).

Based on these results from the tropics coupled with mid-latitude data presented here and in vLR, a number of hypotheses have been put forth in an effort to amend or confirm the original working hypothesis. As was originally suspected, stronger trades appear to decrease SST's in the tropics. What was not anticipated was that stronger trades are, in this case, associated with reduced Gulf Stream velocity. As a possible explanation, it was postulated that reducing SST's over a large area of the Atlantic Ocean current gyre by increased trades increases upwelling, compresses the surface current layer, and causes the whole gyre to expand and slow down due to mass and vorticity conservation. This theory helps to explain the positive SST's seen off the Georgia coast and across the North Atlantic during GB winters (Fig. 12). However, it appears that the observed sea level differences during seesaw winters can be accounted for by steric effects associated with the SST's in the vicinity of the Gulf Stream. This SST pattern seems to be reinforced in the following springs (Fig. 30) with larger areas of positive differences off the east coast and across the North Atlantic. The positive sea level pressure anomaly (Fig. 21) lying over the positive SST differences in the North Atlantic would provide a positive feedback with less clouds, fewer storms, less vertical mixing, more solar heating of the ocean surface and higher SST's.

TABLE 4

SUMMARY OF TROPICAL TELECONNECTIONS DURING GB WINTERS
(VICE VERSA FOR GA WINTERS)

Parameter	Preceding Summers	Preceding Autumns	GB Winters	Following Spring
SLP north of 20°N	no discernable pattern	weak GB, SLP pressure anomaly pattern	stronger subtropical highs; weakened Aleutian low; deepened Icelandic low	weakly stronger subtropical highs
Trade winds	slow building of trades in deep tropics (south of 20°N)	stronger trades in deep tropics	stronger trades throughout tropics (south of 30°N) NE and SE trades highly correlated in seesaw winters, but not in other winters	weakly stronger trades in deep tropics
ITCZ in South Africa			southward shift	
Gulf Stream	weakly stronger →	→	stronger	weakly stronger
SST's	lower SST's in most of tropical Atlantic and Pacific →	→	→	→
subtropical jet			northward shift everywhere except for a southward shift over North Africa	

The postulated expansion of the Hadley cell during GB winters, presumed to be associated with increased trade winds, seems to be associated with an apparent southward shift of the ITCZ in Africa as seen by the precipitation maximum movement in Figure 7, a possible similar southward shift over the Atlantic as seen by areas of positive SST's in the vicinity of the ITCZ cloudiness maximum, and a northward movement of the west wind maximum at 300 mb everywhere in the Northern Hemisphere except over Africa.

The large area of positive SST's in the North Pacific is present to some degree two full seasons before a GB winter, and one season before the first indications of a GB SLP anomaly pattern. If the SST anomaly pattern is already in place, the overlying atmosphere is affected (Davis, 1978) because SST gradients influence atmospheric baroclinic zones, associated areas of cyclogenesis, and storm track positions (Namias, 1975). Therefore a large area of positive SST's in the North Pacific would tend to weaken and steer storms south due to decreased south to north temperature gradient (Namias, 1972). The result could be the negative SLP anomaly seen over the western U.S. and the positive SLP anomalies in the Aleutian area. Contrary to what is happening in the Aleutian area, the SST pattern in the North Atlantic is conducive to deepening the Icelandic low in the mean by steering storms northward as was seen earlier. Therefore, there are an observed deepening of the Icelandic low and an increase in westerlies in the North Atlantic during GB winters.

In any discussion of tropical-midlatitude interactions, the inevitable question of "what comes first" always arises. Here, it appears that the SST pattern has a great deal to do with the onset of

the seesaw winters since the seesaw SST anomaly pattern is present in summers preceding seesaw winters one season prior to the first indications of the seesaw SLP anomaly pattern in autumns preceding seesaw winters. This seems especially plausible in light of Davis' (1978) finding that over the North Pacific autumn and winter SLP anomalies can be predicted from prior SST data. However, the next question is how does the SST anomaly pattern get there in the first place? This cannot be answered conclusively from this study. Namias (1978), in discussing the causes of the GA winter of 1976-77, feels that the SST patterns of that winter were set up a year or more in advance. Lead seasons that far in advance are very difficult to study in the case of the seesaw due to the overlap of some of the consecutively occurring seesaw winters. The fact that SST winters of one mode or the other (GB or GA) tend to occur together over periods of years (vLR, see Fig. 31) tends to lend credence to Namias' hypothesis because one mode of SST pattern would reinforce and maintain seesaw winters of that mode. Similarly, Elsberry and Garwood (1978) show how a persistent SST anomaly pattern can be determined by the frequency and intensity of atmospheric storms during the spring.

A clue as to how an SST pattern of hemispheric extent could be set up was given by Bjerknes (1966). He felt that a breakdown in the southeast trades in the Pacific could cause positive SST anomalies and increase the northeast trades setting off a chain of teleconnections on a hemispheric scale. Even though Bjerknes felt this series of events could take place within one season, this type of interaction remains a possibility here since (1) the strength of the

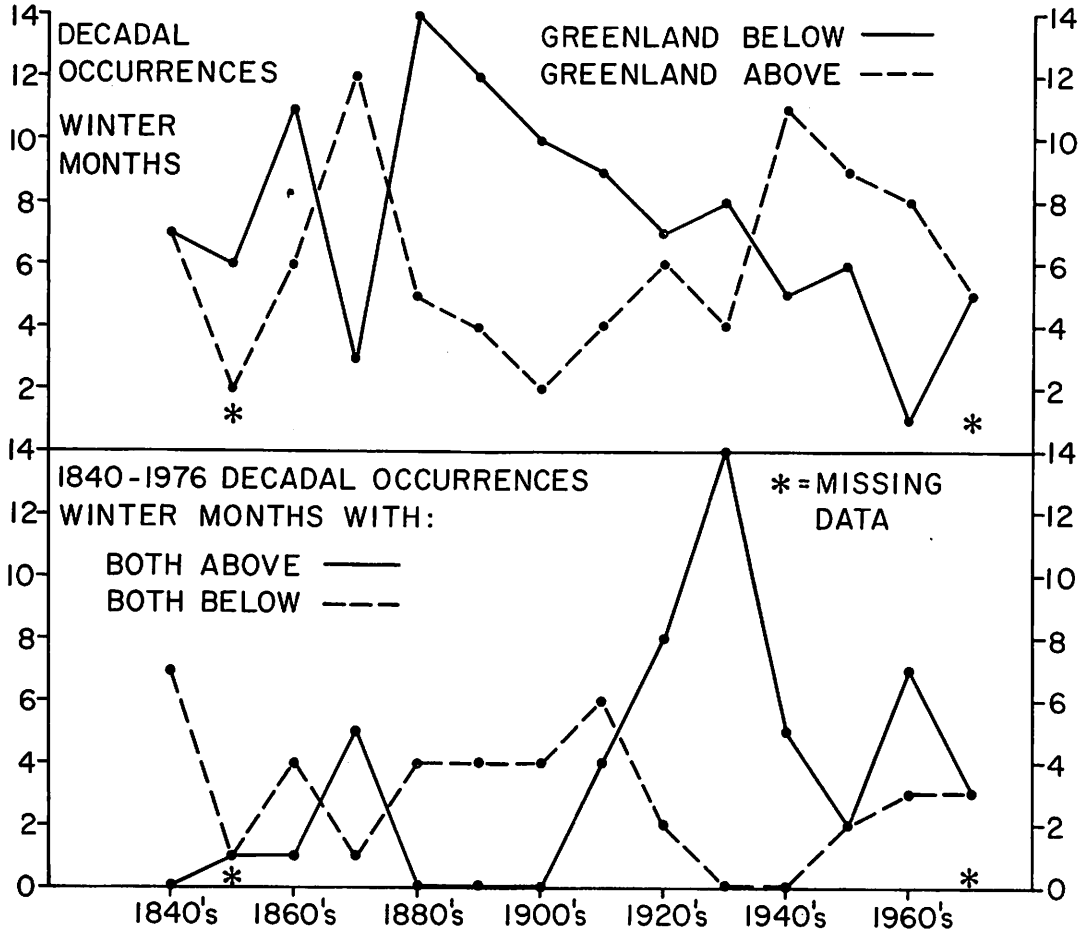

Figure 31. The number of cases per decade of the four temperature categories in winter (DJF). Asterisks denote incomplete decade (after van Loon and Rogers, 1978).

northeast and southeast trades in the Atlantic were shown to be strongly correlated during seesaw winters, but weakly correlated during other winters and (2) northeast trade wind strength in the deep tropics seems to persist two seasons before a seesaw winter. This implies that a breakdown of, say, the southeast trades in the Atlantic a year before a seesaw winter could set up tropical SST patterns that could influence the northeast trades, alter SST's further north, and set up a hemispheric SST pattern over a period of a year culminating in a seesaw winter. Of course it remains a mystery as to why the southeast trades would behave this way in the first place. The eventual answer may lie in the vast data sparse areas of the southern hemispheric oceans.

It was the original intent of this study to investigate the extent to which processes taking place in the tropics could be linked directly to a major mode of midlatitude circulation called the "Greenland seesaw". A number of direct links have been identified, and several processes have been hypothesized to explain these teleconnections. An interesting application of these results would be to see if a general circulation model could duplicate the hemispheric patterns observed during seesaw winters using seesaw boundary conditions to initialize the model. This type of interaction between empirical and theoretical studies has begun to be tried with recent attempts to model the Walker Circulation (Julian and Chervin, 1978; McWilliams and Gent, 1978). In any event, the vital role the tropics play in determining midlatitude circulation has been underscored, and it is hoped that future research will either verify or alter the hypotheses put forth in this study as more and better tropical data are made available.

BIBLIOGRAPHY

Barnett, T. P., 1977: The principal time and space scales of the Pacific trade wind fields. J. Atmos. Sci., 34, 221-236.

Barry, R. G., 1971: Appendix: An introduction to numerical and mechanical techniques. F. J. Monkhouse and H. R. Wilkinson, Maps and Diagrams, London: Methuen, 472-512.

Bjerknes, J., 1969: Atmospheric teleconnections from the equatorial Pacific. Mon. Wea. Rev., 97, 163-172.

_____, 1966: A possible response of the atmospheric Hadley circulation to equatorial anomalies of ocean temperature. Tellus, 18, 820-828.

_____, 1960: Ocean temperatures and atmospheric circulation. WMO Bulletin, XI, 151-157.

British Meteorological Office, 1978: Analysis of historic sea surface temperature data. Ocean Modelling, 14, DAMTP, Cambridge, England.

Brooks, C. F., 1931: Varying trade winds change Gulf Stream temperatures. Gerlands Beiträge zur Geophysik, 34, 400-408.

Brooks, C. E. P., and N. Carruthers, 1953: Handbook of Statistical Methods in Meteorology. Gov't Printing Office, London.

Brown, P. R., 1963: Arid Zone Research. V. 20, Changes of Climate, UNESCO.

Bunker, A. F., 1976: Computations of surface energy flux and annual air-sea interaction cycles of the North Atlantic Ocean. Mon. Wea. Rev., 104, 1122-1140.

_____, and L. V. Worthington, 1976: Energy exchange charts of the North Atlantic Ocean. Bull. Amer. Meteor. Soc., 57, 670-678.

Bryan, K., and M. D. Cox, 1972: An approximate equation of state for numerical models of ocean circulation. J. Phys. Oceanog., 2, 510-514.

Chase, J., 1954: A comparison of certain North Atlantic wind, tide gauge and current data. J. Marine Res., 13, 22-31.

Chervin, R. M., W. M. Washington, and S. H. Schneider, 1976: Testing the statistical significance of the response of the NCAR GCM to north Pacific Ocean surface temperature anomalies. J. Atmos. Sci., 33, 413-423.

Crutcher, H. L., and J. M. Meserve, 1970: Selected Level Heights, Temperatures, and Dew Points for the Northern Hemisphere. Naval Weather Service Command, U.S. Government Printing Office, Washington, D.C.

Davis, R. E., 1978: Predictability of sea level pressure anomalies over the north Pacific Ocean. J. Phys. Oceanog., 8, 233-246.

_____, 1976: Predictability of sea surface temperature and sea level pressure anomalies over the north Pacific Ocean. J. Phys. Oceanog., 6, 249-266.

Doberitz, R., 1968: Cross spectrum analysis of rainfall and sea temperatures at the equatorial Pacific Ocean. Bonner Meteor. Abhandl., 8.

Emery, W. J., 1976: The role of vertical motion in the heat budget of the upper northeastern Pacific Ocean. J. Phys. Oceanog., 6, 299-305.

Fairbridge, R. W., and O. A. Krebs, Jr., 1962: Sea level and the Southern Oscillation. Geophys. J., 6, 532-545.

Flohn, H., and H. Fleer, 1975: Climatic teleconnections with the equatorial Pacific and the role of ocean/atmosphere coupling. Atmosphere, 13, 96-109.

_____, J. Henning, and H. C. Korff, 1965: Studies on the water vapor transport over Northern Africa. Bonner Meteor. Abhandl., 5, 36-48.

Fuglister, F. C., 1951: Annual variations in current speeds in the Gulf Stream system. J. Marine Res., 10, 1-40.

_____, 1947: Average monthly sea surface temperatures of the western North Atlantic Ocean. Pap. Phys. Oceanog. Meteor., 10, 25.

Griffiths, J. F., 1972: Climates of Africa. World Survey of Climatology. Volume 10. London: Elsevier, 604 pp.

Hastenrath, S., 1977: Hemispheric asymmetry of oceanic heat budget in the equatorial Atlantic and Eastern Pacific. Tellus, 29, 523-529.

_____, 1976: Variations in low-latitude circulation and extreme climatic events in the tropical Americas. J. Atmos. Sci., 33, 202-215.

_____, and P. J. Lamb, 1978: Heat Budget Atlas of the Tropical Atlantic and Eastern Pacific Oceans. The University of Wisconsin Press, 104 pp.

Hastenrath, S., and P. J. Lamb, 1977: Climatic Atlas of the Tropical Atlantic and Eastern Pacific Oceans. The University of Wisconsin Press, 112 pp.

_____, and P. J. Lamb, 1977: Some aspects of circulation and climate over the eastern equatorial Atlantic. Mon. Wea. Rev., 105, 1019-1023.

Haworth, C., 1978: Some relationships between sea surface temperature anomalies and surface pressure anomalies. Quart. J. Royal Meteor. Soc., 104, 131-146.

Hellerman, S., 1965: Computation of wind stress fields over the Atlantic Ocean. Mon. Wea. Rev., 93, 239-294.

Hickey, B., 1975: The relationships between fluctuations in sea level, wind stress, and sea surface temperature in the equatorial Pacific. J. Phys. Oceanog., 5, 460-475.

Holton, J. R., 1972: An Introduction to Dynamic Meteorology. Academic Press: New York.

Houghton, D. D., J. E. Kutzbach, M. McClintock, and D. Suchman, 1974: Response of a general circulation model to a sea temperature perturbation. J. Atmos. Sci., 31, 857-868.

Jackson, S. P., 1961: Climatological Atlas of Africa, Government Printer, Pretoria.

Jenkins, G. M., and D. G. Watts, 1968: Spectral Analysis and its Applications. San Francisco: Holden-Day.

Julian, P. R., and R. M. Chervin, 1978: A study of the Southern Oscillation and Walker Circulation phenomenon. Mon. Wea. Rev., in press.

Kidson, J. W., 1977: African rainfall and its relation to the upper air circulation. Quart. J. Royal Meteor. Soc., 103, 441-456.

_____, D. G. Vincent, and R. E. Newell, 1969: Observational studies of the general circulation of the tropics: long term mean values. Quart. J. Royal Meteor. Soc., 95, 258-287.

Kraus, E. B., 1977: Subtropical droughts and cross-equatorial energy transports. Mon. Wea. Rev., 105, 1009-1018.

_____, 1977: Seasonal excursion of intertropical convergence zone. Mon. Wea. Rev., 105, 1052-1055.

Krishnamurti, T. N., 1961: The subtropical jet stream of winter. J. Meteor., 18, 172-191.

_____, 1961: On the role of the subtropical jet stream of winter in the atmospheric general circulation. J. Meteor., 18, 657-670.

Krueger, A. F., and J. S. Winston, 1975: Large scale circulation anomalies over the tropics during 1971-72. Mon. Wea. Rev., 103, 465-473.

Kutzbach, J. E., 1970: Large scale features of monthly mean northern hemisphere anomaly maps of sea level pressure. Mon. Wea. Rev., 98, 708-716.

_____, R. M. Chervin, D. D. Houghton, 1977: Response of the NCAR GCM to prescribed changes in ocean surface temperature, Part 1. Mid-latitude changes. J. Atmos. Sci., 34, 1200-1213.

Lamb, P. J., 1978: Case studies of tropical Atlantic surface circulation patterns during recent sub-Saharan weather anomalies: 1967 and 1968. Mon. Wea. Rev., 106, 482-491.

_____, 1977: On the surface climatology of the tropical Atlantic. Archiv. Meteor. Geophysik Bioklim., B25, 21-31.

Lighthill, M. J., 1969: Dynamic response of the Indian Ocean to onset of southwest monsoon. Philos. Trans., A265, 45-92.

Lisitzin, E., J. G. Pattullo, 1961: The principal factors influencing the seasonal oscillation of sea level. J. Geophys. Res., 66, 845-852.

Madden, R. A., 1976: Estimate of the natural variability of time-averaged sea-level pressure. Mon. Wea. Rev., 104, 942-952.

McCreary, J., 1976: Eastern tropical ocean response of changing wind systems: with application to El Niño. J. Phys. Oceanog., 6, 632-645.

McKee, W. D., 1971: A note on the sea level oscillation in the neighborhood of the Drake Passage. Deep-Sea Res., 18, 54-549.

McWilliams, J. C., and P. R. Gent, 1978: A coupled air and sea model for the tropical Pacific. J. Atmos. Sci., 35, 962-989.

Montgomery, R. B., 1938: Fluctuations in monthly sea level on eastern U.S. coast as related to dynamics of western North Atlantic Ocean. J. Marine Res., 1, 165-185.

Munk, W. H., 1950: On the wind driven ocean circulation. J. Meteor., 7, 79-93.

Murray, R., 1960: Mean 200 millibar winds at Aden in January 1958. Meteor. Mag., 89, 156.

Namias, J., 1978: Multiple causes of the North American abnormal winter 1976-77. Mon. Wea. Rev., 106, 279-295.

_____, 1975: Stabilization of atmospheric circulation patterns by SST. J. Marine Res., 33, 54-60.

Namias, J., 1973: Response of the equatorial counter-current to the subtropical atmosphere. Science, 181, 1244-1245.

_____, 1972: Experiments in objectively predicting some atmospheric and oceanic variables for the winter of 1971-72. J. Appl. Meteor., 11, 1164-1174.

_____, 1969: Seasonal interactions between the North Pacific Ocean and the atmosphere during the 60's. Mon. Wea. Rev., 97, 173-192.

_____, 1964: Seasonal persistence and recurrence of European blocking during 1958-1960. Tellus, 3, 394-407.

_____, 1959: Recent seasonal interaction between north Pacific waters and the overlying atmospheric circulation. J. Geophys. Res., 64, 631-646.

Neumann, G., 1956: Notes on the horizontal circulation of ocean currents. Bull. Amer. Meteor. Soc., 37, 96-100.

Newell, R. E., J. W. Kidson, D. G. Vincent, and G. J. Boer, 1974: The General Circulation of the Tropical Atmosphere and Interactions with Extratopical Latitudes, Vol. 2. M.I.T. Press, 371 pp.

Nicholls, N., 1977: Tropical-extratropical interactions in the Australian region. Mon. Wea. Rev., 105, 826-832.

Nieuwolt, S., 1977: Tropical Climatology. New York: Wiley.

Niiler, P. P., and W. S. Richardson, 1973: Seasonal variability of the Florida current. J. Marine Res., 31, 144-167.

Palmén, E., and C. W. Newton, 1969: Atmospheric Circulation Systems, their Structure and Physical Interpretation. Academic Press, 603 pp.

Pattullo, J. G., Seasonal changes in sea level. In The Sea, Vol. II. M. N. Hill, ed., New York: Interscience Publishers.

_____, W. Munk, R. Nevelle, and E. Strong, 1955: The seasonal oscillation in sea level. J. Marine Res., 14, 88-155.

Peixoto, J. P., and G. O. P. Obasi, 1965: Humidity conditions over Africa during the IGY. Sci. Rept. No. 7, Planetary Circulations Project, Dept. of Meteorology, Mass. Inst. of Technology.

Permanent Service for Mean Sea Level, 1977: Monthly and Annual Mean Heights of Sea Level, Vol. 2. North Central and South America. Institute of Oceanographic Sciences. Bedston Observatory, England (printed by Natural Environmental Research Council).

Pittock, A. B., 1973: Global meridional interactions in stratosphere and troposphere. Quart. J. Royal Meteor. Soc., 99, 424-437.

Ramage, C. S., 1977: Sea surface temperature and local weather. Mon. Wea. Rev., 105, 540-544.

_____, 1974: Structure of an oceanic near-equatorial trough deduced from research aircraft traverses. Mon. Wea. Rev., 102, 754-759.

Ratcliffe, R. A. S., and R. Murray, 1970: New lag associations between North Atlantic sea temperature and European pressure applied to longrange weather forecasting. Quart. J. Royal Meteor. Soc., 96, 226-246.

Reiter, E. R., 1978: Long term wind variability in the tropical Pacific, its possible causes and effects. Mon. Wea. Rev., 106, 324-330.

_____, 1978: The interannual variability of the ocean-atmosphere system. J. Atmos. Sci., 35, 349-370.

Riehl, H., 1973: Controls of the Venezuela rainy season. Bull. Amer. Meteor. Soc., 54, 9-12.

Rogers, J. C., and H. van Loon, 1978: The seesaw in water temperatures between Greenland and northern Europe. Part II: Sea ice, sea surface temperatures, and winds. Submitted to Mon. Wea. Rev.

Rowntree, P. R., 1976: Response of the atmosphere to a tropical Atlantic ocean temperature anomaly. Quart. J. Royal Meteor. Soc., 102, 607-625.

_____, 1976: Tropical forcing of atmospheric motions in a numerical model. Quart. J. Royal Meteor. Soc., 102, 583-605.

_____, 1972: The influence of tropical east Pacific Ocean temperatures on the atmosphere. Quart. J. Royal Meteor. Soc., 98, 290-321.

Salmon, R., and M. C. Hendershott, 1976: Large scale air-sea interactions with a simple general circulation model. Tellus, 28, 228-242.

Sawyer, J. S., 1965: Notes on the possible cause of long term weather anomalies. WMO Tech. Note 66. Geneva, 227-248.

Shaw, W. N., 1905: The pulse of the atmospheric circulation. Nature, 21, 175-177.

Stommel, H., 1964: Summary charts of the mean dynamic topography and current field at the surface of the ocean, and related functions of the mean wind-stress. Studies on Oceanography, pp. 53-58.

Stommel, H., 1960: The Gulf Stream. Berkeley, California: Univ. of Cal. Press. 202 pp.

_____, 1953: Examples of the possible role of inertial and stratification in the dynamics of the Gulf Stream system. J. Marine Res., 12, 184-195.

_____, 1951: An elementary explanation of why ocean currents are strongest in the west. Bull. Amer. Meteor. Soc., 32, 21-23.

Sverdrup, H. U., M. W. Johnson, and R. H. Fleming, 1946: The Oceans, Their Physics, Chemistry and General Biology. New York: Prentice-Hall.

Taljaard, J. J., 1972: Synoptic meteorology of the Southern Hemisphere. Meteor. Monographs, 13, 137-211.

_____, 1955: Stable stratification in the atmosphere over southern Africa. Notos, 4, 217-230.

_____, H. van Loon, H. L. Crutcher, and R. L. Jenne, 1969: Climate of the Upper Air, Southern Hemisphere: Vol. 1: Temperatures, Dew Points, and Heights at Selected Pressure Levels. U.S. Dept. of Commerce.

Tanaka, M., B. C. Weare, A. R. Navato, and R. E. Newell, 1975: Recent African rainfall patterns. Nature, 225, 201-203.

Troup, A. J., 1961: Variations in 200 mb flow in the tropics. Meteor. Mag., 90, 162-167.

van Loon, H., 1972: Half yearly oscillations in the Drake Passage. Deep-Sea Res., 19, 525-527.

_____, and J. Williams, 1977: The connection between trends of mean temperature and circulation at the surface: Part IV. Mon. Wea. Rev., 105, 636-647.

_____, and J. C. Rogers, 1978: The seesaw in winter temperatures between Greenland and Northern Europe. Part I: General description. Mon. Wea. Rev., 106, 296-310.

Washington, W. M., R. M. Chervin, and G. V. Rao, 1977: Effects of a variety of Indian Ocean surface temperature anomaly patterns on the summer monsoon circulation: experiments with the NCAR general circulation model. Pageoph., 115, 1335-1356.

Weinert, R. A., 1968: Statistics of the subtropical jet stream over the Australian region. Aust. Meteor. Mag., 16, 137-148.

Willett, H. C., 1949: Long period fluctuations of the general circulation of the atmosphere. J. Meteor., 6, 34-50.

Wyrtki, K., 1975: El Niño -- the dynamic response of the equatorial Pacific Ocean to atmospheric forcing. J. Phys. Oceanog., 5, 572-584.

_____, 1975: Fluctuations of the dynamic topography of the Pacific Ocean. J. Phys. Oceanog., 5, 450-459.

_____, 1974: Equatorial currents in the Pacific 1950-1970 and their relations to the trade winds. J. Phys. Oceanog., 4, 372-380.

_____, 1973: Teleconnections in the equatorial Pacific Ocean. Science, 180, 66-68.

_____, 1965: The annual and semi-annual variations of sea surface temperature in the North Pacific Ocean. Limnol. Oceanog., 10, 307-313.

APPENDICES

APPENDIX A

Equations

a. Statistical equations

Several programs have been developed during the course of this study that use statistical equations to evaluate relationships between sets of data; a list of the programs appears in Appendix B. The following is a list of the equations in the computational form in which they appear in those programs.

t value:

$$t = \frac{\overline{x_1} - \overline{x_2}}{\sqrt{\frac{1}{n_1} + \frac{1}{n_2}} \sqrt{\frac{\left[\sum x_{1i}^2 - \frac{(\sum x_{1i})^2}{n_1}\right] + \left[\sum x_{2i}^2 - \frac{(\sum x_{2i})^2}{n_2}\right]}{n_1 + n_2 - 2}}}$$

where x_1 and x_2 are 2 sets of data, n_1 and n_2 are the number of observations in each set, and x_{1i} and x_{2i} are individual observations within each set.

note: the computational t value equation was developed from the general t value equation of the form given by Barry (1971):

$$t - \frac{\overline{x_1} - \overline{x_2}}{\sqrt{\frac{\sigma_1^2}{n_1 - 1} + \frac{\sigma_2^2}{n_2 - 1}}}$$

where x_1 and x_2 are two sets of data, n_1 and n_2 are number of observations in each set and σ_1 and σ_2 are standard deviations of each set and where

$$\sigma_i^2 = \frac{\sum(x_i - \bar{x}_i)^2}{n_i}$$

correlation coefficient:

$$r_{(x_{1i}\ x_2)} = \frac{\sum\left(\overline{x_{1i}\ x_{2i}} - \bar{x}_{1i}\ \bar{x}_{2i}\right)}{\sqrt{\sum\left(\overline{x_{1i}^2} - \bar{x}_{1i}^2\right) \cdot \sum\left(\overline{x_{2i}^2} - \bar{x}_{2i}^2\right)}}$$

where x_1 and x_2 are two sets of data and x_{1i} and x_{2i} are individual observations within each set.

note: the computational correlation coefficient was developed from the equation for the general correlation coefficient between two variables x and y:

$$r_{xy} = \frac{\sum\left[(X - \bar{X})(Y - \bar{Y})\right]}{\sqrt{\left[\sum(X - \bar{X})^2 \cdot \sum(Y - \bar{Y})^2\right]}}$$

as given by Brooks and Carruthers (1953).

To arrive at the correlation coefficient computationally, first compute covariances since

$$\text{correlation } (x_i, x_j) = \frac{\text{covariance } (x_i, x_j)}{\sqrt{\text{covariance } (x_i, x_i)\ \text{covariance } (x_j, x_j)}}$$

It is necessary to accumulate sums of products and squares of the covariance terms:

$$\text{covariance} = \overline{\left(x_i - \bar{x}_i\right)\left(x_j - \bar{x}_j\right)}$$

$$= \overline{x_i x_j} - \overline{\bar{x}_i x_j} - \overline{x_j \bar{x}_j} + \overline{\bar{x}_i \bar{x}_j}$$

the mean of a mean is simply that

$$\text{mean} \quad \left(\text{i.e. } \bar{\bar{x}}_i = \bar{x}_i\right), \text{ and}$$

$$= \overline{x_i x_j} - \bar{x}_i \bar{x}_j - \bar{x}_i \bar{x}_j + \bar{x}_i \bar{x}_j$$

$$\therefore \text{covariance} = \overline{x_i x_j} - \bar{x}_i \bar{x}_j$$

If $j = i$ [as encountered in computing $\text{cov}\left(x_i x_i\right)$ for example] then

$$\text{covariance} = \overline{x_i x_i} - \bar{x}_i \bar{x}_i$$

$$X = \overline{x_i^2} - \bar{x}_i^2$$

where X is called the variance which is the covariance with subscripts equal.

<u>significance test for correlation coefficient</u>:

$$95\% \text{ limit} = \frac{1.96}{\sqrt{N}}$$

$$99\% \text{ limit} = \frac{2.58}{\sqrt{N}}$$

where N is the number of pairs being correlated (Jenkins and Watts, 1968).

b. Other equations

geostrophic wind:

$$V_g = -\frac{1}{\rho f}\frac{\partial p}{\partial n}$$

where V_g is the computed geostrophic wind blowing perpendicular to n, ρ is air density, f is the Coriolis force, and $\partial p/\partial n$ is the pressure gradient along n (Holton, 1972).

thermal wind

for zonal component u,

$$U_t = -\frac{R}{f}\left(\frac{\partial \bar{T}}{\partial y}\right)_p \ln\left(\frac{p_0}{p_1}\right)$$

where $\bar{T}$ is the mean temperature in the layer between pressure p_0 and p_1, R is the gas constant, f is the Coriolis force (Holton, 1972).

bulk aerodynamic equations

momentum: $\tau = \rho C_D U_{10}^2$

water vapor: $E = \rho C_E (q_s - q_{10}) U_{10}$

sensible heat: $S = \rho C_H c_p (T_s - T_{10}) U_{10}$

where τ, E and S are averages of momentum, water vapor, and sensible heat; ρ is air density, C_D, C_E and C_H are empirically determined exchange coefficients for momentum, water vapor and sensible heat; U_{10} is the average wind speed at 10 m or ship anemometer level; q_s and q_{10} are averages of mixing ratios of air in contact with salt water and at 10 m of deck level; and T_s and T_{10} are average temperatures of sea surface and air at the upper level (Bunker, 1976).

net radiational exchange

$$R = Q\left(1 - \alpha\right) - IR$$

where Q is incoming solar radiation, α is albedo of the ocean surface and IR is outgoing infrared radiation (Bunker, 1976).

APPENDIX B

Computer programs

The following are brief descriptions of the computer programs developed and written for this study. Listings of these programs are available from the author.

(1) PCORR: takes SLP for a given set of individual months and correlates a desired point of the pressure grid to all other points and produces a spatial correlation field.

(2) SPCORR: same as PCORR except for winters.

(3) WINDCOR (a): for individual months -- computes U and V component geostrophic winds from SLP grid, then correlates desired key grid point to all other points producing a spatial correlation field similar to PCORR and SPCORR.

(4) WINDCOR (b): same as WINDCOR (a) except for winters.

(5) SSTEMP (a): uses 5^{o} grid of sea surface temperatures and differences two sets of individual months; also computes t values for individual months.

(6) SSTEMP (b): same as SSTEMP (a) except for winters.

(7) SSTEMP (c): same as SSTEMP (b) except for seasons other than winter.

(8) SSTEMP (d): produces a count of individual observations per 5^{o} square.

(9) UPLEVS: correlates winter 700 mb temperature gradients computed and averaged from tape of 5^{o} latitudinal monthly 700 mb temperatures with upper level u winds computed and averaged from a tape of 5^{o} monthly upper level heights.

(10) TGRAD7: computes 700 mb temperature gradients from seasonal 5^{o} 700 mb temperatures, differences 2 sets of gradients from desired seasons, and performs a t test on the differences.

APPENDIX C

Method for computing geostrophic wind using pressure values from a pair of stations

Given a pair of stations, A and B, it is desired to compute the resultant geostrophic wind (V_g) blowing perpendicular to the axis between those two stations using SLP data from each station.

The general geostrophic wind equation given in Appendix A is

$$V_g = -\frac{1}{\rho f}\frac{\delta p}{\delta n}$$

The form used in this computation is

$$V_g = \frac{1}{\rho f}\frac{\Delta p}{\Delta n}$$

where Δp is the pressure difference between stations A and B, Δn is the geostrophic distance between A and B, ρ is air density and taken to be 1.225×10^{-3} g/cm^3; and f is the Coriolis force given by

$$f = 2\,\Omega \sin \phi$$

where Ω is the angular velocity of the earth $(7.292 \times 10^{-5}\,\text{sec}^{-1})$, and ϕ is the latitude of the midpoint of the axis between A and B which, if ϕ and λ are latitude and longitude, lies at $1/2(\phi_B - \phi_A)$ (see figure below)

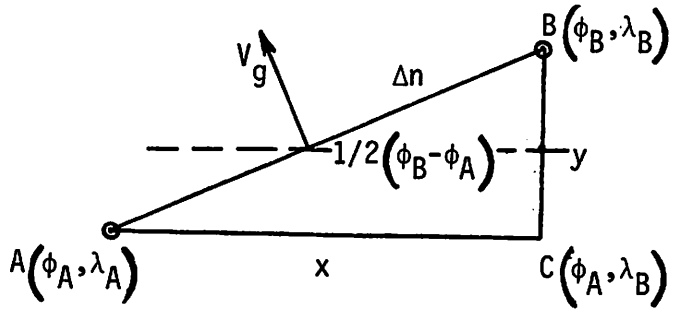

To compute the linear distance Δn from station A to station B, the length of the sides of the triangle ABC must be determined. Length of side AC is given by

$$x = \frac{2 \pi R \left(\lambda_A - \lambda_B\right)\left(\cos \phi_A\right)}{360}$$

where R, the radius of the earth, is taken to be 6.371229×10^8 cm. The length of side BC is given by

$$y = \frac{2 \pi R \left(\phi_B - \phi_A\right)}{360}$$

The distance from A to B $\left(\Delta n\right)$ can then be determined by

$$\Delta n = \sqrt{x^2 + y^2}$$

After values of Δp are computed from station records, all the preceding quantities are substituted into the geostrophic wind equation and the resultant geostrophic wind is computed.

APPENDIX D

Sea surface temperature observation density for 45 seesaw winters, 1854-1968.